Dear Editor and reviewers,

Thank you for all the constructive comments on our manuscript. We feel sure that addressing the comments will improve the quality of the paper. Below, we provide our responses to all three reviewer comments.

Best Wishes

Hansruedi Maurer (on behalf of the author team)

Reviewer 1 (Ben Pelto)

General comments

- ***Availability of code and data***
  We plan to make the GlaTE Matlab scripts publically available on GitHub. Likewise, we will upload the data sets employed in the paper on this platform. This will allow reproducing all our results, and we hope that the codes will be helpful for other data sets.
- ***Accuracy of H-GPR ice thickness estimates***
  Indeed, the accuracy of the H-GPR thickness estimates is critical for our algorithm. As noted correctly by the reviewer, the literature offers quite a range of thickness estimates. We have re-evaluated our data and concluded that a depth-dependent accuracy (i.e., percentage error) would be a better option. A reasonable choice for our data sets is 5%, that is, an accuracy of 5 m would correspond to a thickness of 100 m. When available, it would be straightforward to consider individual accuracy estimates for the individual data points. In the modified manuscript we include a more detailed discussion on this topic.

Specific comments

- ***Editiorial comments***
  We have addressed all editorial comments
- ***Sampling of DTM***
  Yes, the DTM is sampled on R, as it was indicated on line 105
- ***Mass balance estimates***
  Yes, the results are in broad agreement with typical values obtained in this region
- ***Table with glaciers***
  The revised paper includes a table with the important characteristics of the glaciers considered
- ***Merging of different campaigns***
  An earlier version of the manuscript included data sets of merged campaigns. However, we decided to show only data sets that were acquired in the framework of a single campaign, to avoid the problem of the ongoing melt. The statement about the merged data set was just a remnant from the earlier draft, and we have removed it in the revised version.
- ***Table with ice thickness estimates***
  Since we make the data sets publically available, we don’t think that such a table is necessary
- ***SOED and crossing profiles***
  We added additional text in the revised manuscript to address this issue

- ***Adding data to GlaThiDa***
  Our measurements in Switzerland until 2015 are covered in the GlaThiDa 3.0 release, and we intend to provide an update with the next release

Reviewer 2 (Douglas Brinkerhoff)

General comments

- ***Novelty of approach***
  We do not claim that the ice thickness estimation approach within GlaTE is novel. As indicated on line 112ff, any of the algorithms described in the literature can be incorporated. The novelty lies rather in the consideration of the uncertainties of the H-GPR measurements, and in the formulation in form of a sparse system of linear equations, which allows incorporating any further constraints. In the revised manuscript, we make this more obvious in the abstract.
- ***Choice of weighting parameters λ_1 to λ_4***
  We agree with Reviewers 2 and 3 that the discussion on the choice of the weighting parameters may be confusing. Based on their comments, we re-thought the strategy for choosing λ_1 *to* λ_4. The revised manuscript includes a more detailed description. In brief, we fix λ_3 to a constant value. This parameter has very little effect on the inversion result. Next, we perform a series of inversions with different λ_1/λ_2 ratios (remain fixed during a single inversion run). During each inversion run, the smoothing parameter λ_4 is gradually lowered, until a prescribed percentage (e.g., 95%) of the GPR data is fitted with the prescribed accuracy. When the λ_1/λ_2 ratio is getting too small, the inversion algorithm fails to match the GPR data, even when $\lambda_4 = 0$. The lowest ratio, which allows to fit the GPR data, is finally chosen. This procedure (i) allows to fit the GPR data with a prescribed accuracy (no overfitting), (ii) maximizes the contribution of the glaciological constraints and (iii) minimizes the influence of the (unphysical) smoothing constraints.

  Reviewers 2 and 3 suggested cross validation methods for identifying optimal weighting parameters. This is potentially an interesting option, but we judge the procedure outlined above to be physically more meaningful and computationally cheaper.
- ***Choice of α parameter***
  Reviewer 2 is right. It makes conceptually much more sense to minimize the squared differences between observed and modelled thicknesses. We changed the manuscript accordingly and recomputed the three test cases. Interestingly, the α values, obtained with the new procedure, are very similar to the old values.
- ***Choice of lines during SOED procedure***
  The choice of the lines is influenced by a plethora of factors. However, the procedure does not consider (explicitly) the amount of crossing profiles, which could be advantageous for cross-checks. We have added a more detailed explanation on this topic.

Reviewer 3 (Fabien Maussion)

General comments

- ***Choice of regularization parameters***
  See response to Reviewer 2 on this topic.
- ***Objective assessment of GlaTE performance***
  We agree that our statement concerning the performance of GlaTE is somewhat weak. We have participated in the ITMIX2 initiative, where numerous approaches were compared in form of blind tests. Evaluation of ITMIX2 is still in progress, but we make a reference to this initiative, which is certainly a good measure for the performance of GlaTE.
- ***Code and data availability***
  See response to Reviewer 1 on this topic

Specific comments

- ***Flowsheds***
  We also expected discontinuities between flowsheds, but surprisingly this was not the case.
- ***Apparent mass balance computation and glacier cluster***
  More explanation were added to the text
- ***Lower boundary of Di***
  We followed the approach of Clarke et al. (2013)
- ***θ vs ϕ***
  This is the same quantity. The typo was corrected
- ***α parameter***
  α accounts for the uncertainties of all multiplicative factors in Equation (5), also including *A*.
- ***mean(abs(diff()) issue***
  See corresponding response to Reviewer 2
- ***LSQR***
  The system of equations includes ~300,000 rows and ~90,000 columns. Due to the sparseness of the system matrix, the LSQR algorithm requires only about 2 seconds on a standard PC with a 3 GHz processor. However, due to the adjustments of the smoothing parameter λ_4, the system of equations needs to be solved several times during an inversion run.
- ***Figure 1***
  The figure caption (resp. the figure itself) was corrected
- ***Flight time to next profile***
  Yes, this is correct. We did not account for the transition time. This was already mentioned on line 590.
- ***Statistical analysis for determining α***
  During the next few months, we will analyze a very large data set acquired over all significant glaciers in Switzerland. We hope that we can prove you to be wrong …..

Glacier thickness estimations of alpine glaciers using data and modeling constraints

Lisbeth Langhammer[1]
Melchior Grab[1,2]
Andreas Bauder[2]
Hansruedi Maurer[1*]

[1] Institute of Geophysics, ETH Zurich, Switzerland
[2] Laboratory of Hydraulics, Hydrology and Glaciology (VAW), ETH Zurich, Switzerland
[*] Corresponding author (*hansruedi.maurer@erdw.ethz.ch*)

Abstract

Advanced knowledge of the ice thickness distribution within glaciers is of fundamental importance for several purposes, such as water resource management and studying the impact of climate change. Ice thicknesses can be modeled using ice surface features, but the resulting models can be prone to considerable uncertainties. Alternatively, it is possible to measure ice thicknesses, for example, with ground-penetrating-radar (GPR). Such measurements are typically restricted to a few profiles, with which it is not possible to obtain spatially unaliased subsurface images. We developed the Glacier Thickness Estimation algorithm (GlaTE), which optimally combines modeling results and measured ice thicknesses in an inversion procedure to obtain overall thickness distributions. GlaTE offers the flexibility to add any existing modeling algorithm, and any further constraints can be added in a straightforward manner. Furthermore, it accounts for the uncertainties associated with the individual constraints. Properties and benefits of GlaTE are demonstrated with three case studies performed on different types of alpine glaciers. In all three cases, subsurface models could be found that are consistent with glaciological modeling and GPR data constraints. Since acquiring GPR data on glaciers can be an expensive endeavor, we additionally employed elements of sequential optimized experimental design (SOED) for determining cost-optimized GPR survey layouts. The calculated benefit-cost curves indicate that a relatively large amount of data can be acquired, before redundant information is collected with any additional profiles and it becomes increasingly expensive to obtain further information. ~~Only at one out of the three test sites this level was reached.~~

1 Introduction

Estimating the amount of the glacier ice around the globe is crucial, for example, for sea-level predictions, securing fresh water ~~recourses~~resources, designing hydropower facilities in high-alpine environments, and predicting the occurrence of glacier-related natural hazards. For estimating the overall glacier ice mass and its local distribution, (i) knowledge of the glacier outline, (ii) its surface topography and (iii) the underlying bedrock topography is required. The first two quantities can be observed with aerial and satellite imagery, but the bedrock topography is more difficult to determine.

The conceptually simplest option includes drilling boreholes through the glacier ice (e.g., Iken, 1988). This approach offers ground-truth information, but only a very sparse observation grid can be obtained with realistic efforts. Therefore, geophysical methods have been employed for obtaining more detailed information. Due to the very high electrical resistivity of glacier ice and the relatively high electromagnetic impedance contrast between ice and bedrock material, ground-penetrating-radar (GPR) techniques, also referred to as radio-echo-sounding~~ (RES)~~, have been the primary choice for such investigations (e.g., Evans, 1963). GPR data can either be acquired ground-based (e.g., Watts and England, 1976), or, more efficiently, using fixed-wing airplanes (e.g., Steinhage et al., 1999) or helicopters (e.g., Rutishauser et al., 2016).

Despite the powerful capabilities of modern GPR acquisition systems, it is still beyond any practical limits to acquire spatially un~~-~~aliased 3D data sets. GPR data are therefore collected only along a sparse network of profiles, which leaves considerable uncertainties in the regions between the profiles.

To address this problem, glaciological modeling techniques have been established to relate observable surface parameters to the thickness distribution of ice. One of the earliest concepts was published by Nye (1952). He established a simple relationship between the surface slope and ice thickness. During the past decades, more sophisticated ice thickness modeling techniques have emerged rapidly. Various glaciological constraints, such as mass conservation and/or the relation between basal shear stress and ice thickness, were considered (e.g., Farinotti et al., 2009;Huss and Farinotti, 2012;Clarke et al., 2013;Linsbauer et al., 2012;Morlighem et al., 2011). See Farinotti et al. (2017) for a more complete review of most of the approaches published to date.

Due to inaccuracies of the observed data (GPR measurements, surface topography, etc.) and/or inadequacies of the modeling approaches, modeled ice thicknesses cannot be expected to be perfect. This can be considered by formulating ice thickness estimation as an optimization problem, in which the discrepancies between observed and predicted data are minimized (e.g., Morlighem et al., 2014). In this contribution, we follow an approach similar to Morlighem et al. (2014), but with a different implementation. We introduce the general framework of Glacier Thickness Estimation (GlaTE), with which modeling and data constraints can be combined in an appropriate fashion. After introducing the underlying theory, we demonstrate the performance of the GlaTE inversion procedure with three case studies. In the second part of the paper, we employ elements of GlaTE to address the experimental design problem. Here, we seek a measured data set that offers maximum information content at minimal costs. For that purpose, we consider sequentially optimized experimental design (SOED) techniques (e.g., Maurer et al., 2017). The paper concludes with a critical review of potential problems and shortcomings of GlaTE and the associated SOED procedures, and we outline options to address these issues and propose useful extensions of the methodology.

2 GlaTE inversion algorithm

2.1. Theory

The basic idea of GlaTE inversions is to combine observable data with glaciological modeling constraints~~,~~. A key feature of the algorithm includes appropriate consideration of~~whereby it is attempted to consider appropriately~~ the uncertainties associated with both constraints~~types of information~~. All constraints are formulated, such that they can be integrated into a single system of equations, which can be solved with an appropriate solver.

The first type of constraints includes the GPR data. They can be written in the form of

(1) $$\mathbf{G}\,\mathbf{h}^{\mathbf{est}} = \mathbf{h}^{\mathbf{GPR}} \ ,$$

where $\mathbf{h}^{\mathbf{est}}$ is a vector including the unknown (*est*imated) ice thicknesses at M locations (typically defined on a regular grid R on a glacier), and $\mathbf{G}$ is a $N^{GPR} \times M$ matrix with ones in its main diagonal and zeros everywhere else (N^{GPR} = number of available GPR data points, M = number of elements in $\mathbf{h}^{\mathbf{est}}$). The vector $\mathbf{h}^{\mathbf{GPR}}$ of length N^{GPR} includes the GPR-based thickness estimates. Since the GPR data usually do not coincide with the grid points of R, the values $\mathbf{h}^{\mathbf{GPR}}$ are obtained by interpolating or extrapolating the GPR data to the nearest grid points of R.

Next, we consider glaciological modeling constraints. In principle, any of the algorithms proposed in the literature can be employed. Here, we follow closely the approach described in Clarke et al. (2013). Input data include a digital terrain model (DTM, defined on R) and the glacier outline.

First, the glacier area is subdivided into so-called flowsheds using the Matlab TOPO-Toolbox (Schwanghart and Kuhn, 2010). The subsequent procedure is applied to each flowshed individually (see comments in Clarke et al. (2013) for more information on the flowshed subdivision).

Next, the apparent mass-balance, defined as

(2) $$\tilde{\mathbf{b}} = \dot{\mathbf{b}} - \frac{\partial \mathbf{h}}{\partial t} \ ,$$

with $\dot{\mathbf{b}}$ being the mass balance rate, and $\frac{\partial \mathbf{h}}{\partial t}$ the thickness change rate, is either determined by measuring $\dot{\mathbf{b}}$ and $\frac{\partial \mathbf{h}}{\partial t}$, or computed via the condition

(3) $$\int_{\Omega_G} \tilde{\mathbf{b}} = 0 \ ,$$

where Ω_G denotes the glacier area (see Farinotti et al. (2009) for more details). In a next step, the flowsheds are partitioned into a prescribed number of elevation zones D_i ($i = 1 \ldots$ *number of elevation zones*), for which the ice discharge Q_i through its lower boundary is computed using

(4) $$Q_i = \int_{\Omega_{D_i}} \tilde{\mathbf{b}} \ ,$$

where Ω_{D_i} is the area of zone D_i. Following Clarke et al. (2013), the basal shear stress τ can then be obtained via the relationship

(5) $$\boldsymbol{\tau} = \left[\frac{(n+2)\rho g \sin(\phi)^2 \xi \mathbf{q}}{2A} \right]^{1/(n+2)}$$

The parameters n, ρ, g and A denote the exponent of Glen's flow law, ice density, gravity acceleration and creep rate factor, respectively (e.g., Cuffey and Patterson, 2010). The factor ξ denotes the creeping contribution (relative to basal sliding) to the ice flux $(0 < \xi < 1)$, and $\mathbf{q}$ is the specific ice discharge $q_i = \bar{Q}_i / l_i$, where l_i is the length of the lower boundary of D_i, and $\bar{Q}_i$ is the average of Q_i within D_i. Likewise, the angle ϕ represents the surface slope averaged along the lower boundary of D_i.

As outlined in Kamb and Echelmeyer (1986), the physics of ice flow can be incorporated into the modeling procedure by applying "longitudinal averaging" of the shear stress (i.e., along the flow direction). We apply this procedure to the results obtained with Equation (5). Finally, the ice thicknesses $\hat{\mathbf{h}}^{\mathbf{glac}}$ (*glac* stands for glaciological modeling constraints) are obtained using

(6) $$\hat{\mathbf{h}}^{\mathbf{glac}} = \frac{\boldsymbol{\tau}^*}{\rho g \sin(\phi)} \ ,$$

where $\boldsymbol{\tau}^*$ denotes the basal shear stress after longitudinal averaging.

Some of the parameters in Equation (5) may be subject to considerable uncertainties. For example, the parameter ξ is often poorly known, and it is not guaranteed that the values of the parameters A and n, usually taken from the literature, are accurate. Typically, n is reasonablye well constrained, but A can vary over orders of magnitudes. Therefore, the overall magnitudes of $\hat{\mathbf{h}}^{\mathbf{glac}}$ may be significantly over- or under-estimated. This can be considered with an additional factor α_{GPR}, yielding

(7) $$\mathbf{h}^{\mathbf{glac}} = \alpha_{GPR}\hat{\mathbf{h}}^{\mathbf{glac}} .$$

α_{GPR} can be computed with an optimization procedure that minimizes
$$\left\|\mathbf{h}^{\mathbf{GPR}} - \alpha_{GPR}\hat{\mathbf{h}}^{\mathbf{glac}}\right\|^2 .$$

The correction factor α_{GPR} accounts for some inadequacies of Equation (5), but it is still possible that there are systematic differences between $\mathbf{h}^{\mathbf{GPR}}$ and $\mathbf{h}^{\mathbf{glac}}$. To avoid the resulting inconsistencies, we consider not the absolute values $\mathbf{h}^{\mathbf{glac}}$, but the spatial gradients $\nabla\mathbf{h}^{\mathbf{glac}}$ as glaciological constraints, resulting in

(8) $$\mathbf{L}\mathbf{h}^{\mathbf{est}} = \nabla\mathbf{h}^{\mathbf{glac}} ,$$

where **L** is a difference operator of dimension $M \times M$.

Further constraints can be imposed via the glacier boundaries that can be determined from aerial or satellite images or ground observations. They are considered in the form of the equation

(9) $$\mathbf{B}\mathbf{h}^{\mathbf{est}} = 0 ,$$

where **B** is a $M \times M$ matrix with ones at appropriate places in its main diagonal.

Depending on the discretization of the glacier models (i.e., the discretization of *R*), the constraints described above, may allow the resulting system of equations to be solved unambiguously. However, in most cases, there will be still a significant underdetermined component, that is, there will be many solutions that explain the data equally well. This requires regularization constraints to be applied (e.g., Menke, 2012). A common strategy for regularizing such problems is to follow the Occam's principle, which identifies the "simplest" solution out of the many possible solutions (Constable et al., 1987). Here, we define "simplicity" in terms of structural complexity, that is, we seek a smooth model. This can be achieved via a set of smoothing equations of the form

(10) $$\mathbf{S}\mathbf{h}^{\mathbf{est}} = 0 ,$$

where **S** is a $M \times M$ smoothing matrix.

All the constraints can now be merged into a single system of equations

(11) $$\begin{pmatrix} \lambda_1\mathbf{G} \\ \lambda_2\mathbf{L} \\ \lambda_3\mathbf{B} \\ \lambda_4\mathbf{S} \end{pmatrix} \mathbf{h}^{\mathbf{est}} = \begin{pmatrix} \lambda_1\mathbf{h}^{\mathbf{GPR}} \\ \lambda_2\nabla\mathbf{h}^{\mathbf{glac}} \\ 0 \\ 0 \end{pmatrix} ,$$

where the parameters λ_1 to λ_4 allow a weighting according to the confidence into the individual contributions. The dimension of the system of equations in (11) can be very large, but the matrices **G**, **L**, **B** and **S** are all extremely sparse. Therefore, sparse matrix solvers, such as LSQR (Paige and Saunders, 1982) can solve such systems efficiently for $\mathbf{h}^{\mathbf{est}}$. The test data sets, described below, included matrices up to $\sim 320,000 \times 90,000$ elements. The LSQR algorithm for such a matrix required approx. 2 seconds on a standard PC.

A critical part of the GlaTE inversions includes a proper choice of the weighting paramters λ_1 to λ_4. ~~where the parameters λ_1 to λ_4 allow a weighting according to the confidence into individual contributions.~~ Parameter λ_3 is not critical and can be fixed to an appropriate value (e.g., 1.0). The magnitudes of the remaining three parameters must be chosen, such that the system of equations in (11) is solvable. However, it also needs to be considered that ~~all~~ the constraints related to λ_1 and~~,~~ λ_2 ~~and λ_4 may be~~are subject to significant inaccuracies. It is difficult to predict the accuracy of the modeling constraints~~ and to judge the appropriateness of the smoothing constraints~~, but the accuracy of the GPR data constraints, subsequently denoted as $\boldsymbol{\varepsilon}^{\mathbf{GPR}}$, can usually be quantified. Therefore, we have chosen the following strategy.

1. Initially, we set $\lambda_1 = 1$ and choose a low λ_2 value (i.e., a high λ_1/λ_2 ratio). Such a ratio indicates a much higher confidence in the GPR data constraints compared with the glaciological modeling constraints. Furthermore, we choose a large value of λ_4, which is expected to oversmooth the ice thickness estimates.
2. With this choice of parameters, a first GlaTE inversion is carried out, and it is checked, if a prescribed percentage (e.g., 95%) of the estimated thicknesses $\mathbf{h}^{\mathbf{est}}$ matches the GPR data $\mathbf{h}^{\mathbf{GPR}}$ within their accuracy limits $\pm\boldsymbol{\varepsilon}^{\mathbf{GPR}}$.
3. For an overly high value of λ_4, it cannot be expected that the prescribed percentage of matching data can be achieved. Therefore, λ_4 is gradually lowered, until the condition, specified in point 2, is met, or a prescribed lower threshold of $\lambda_4 = \lambda_4^{\min}$ is reached. The final smoothing weight, obtained with this procedure, is denoted as $\bar{\lambda}_4$. Since the λ_1/λ_2 ratio is still large, it is expected that $\bar{\lambda}_4$ is also large, because the modeling constraints do not contribute much to the GlaTE inversion. Essentially, a smooth interpolation of the GPR data between the profile lines is performed.
4. The λ_1/λ_2 ratio is gradually lowered, and step 3 is carried out again (λ_4 is reset to a high initial value). This iterative procedure is repeated until (i)

$\bar{\lambda}_4 = \lambda_4^{\min}$ without reaching the prescribed data match, or (ii) the λ_1 / λ_2 ratio has reached a prescribed lower limit.

With decreasing λ_1 / λ_2 ratios, the importance of the glaciological modeling constraints increases, and the contribution of the smoothing constraints need~~s~~ to be lowered to achieve the prescribed data match. Below a certain λ_1 / λ_2 ratio, it will likely no longer be possible to fit a sufficently large percentage of the data within the limits $\pm \boldsymbol{\varepsilon}^{\mathbf{GPR}}$, even when $\bar{\lambda}_4 = \lambda_4^{\min}$. If this is not the case, the λ_1 / λ_2 ratio could be lowered to an arbitrary low level, but if the confidence in the glaciological modeling constraints is rather limited, it is possible to define a lower threshold, where the GlaTE inversion would stop, even when $\bar{\lambda}_4 > \lambda_4^{\min}$.

With such a strategy, it is possible to achieve several desirable features of glacier thickness estimations, namely

- the GPR data are fitted only within the prescribed accuracy limits, and no overfitting is performed,
- the contribution of the glaciological constraints are maximized, and
- the influence of the (unphysical) smoothing constraints is minimized.

~~Therefore, λ_1, λ_2 and λ_4 have to be chosen, such that the discrepancy of the GPR data $\left(\left\|\mathbf{G}\,\mathbf{h}^{\mathrm{est}} - \mathbf{h}^{\mathbf{GPR}}\right\|\right)$ is of the order of $\boldsymbol{\varepsilon}^{\mathbf{GPR}}$, and the GPR data are thus neither under- nor over-fitted. We have implemented this by choosing the magnitudes of λ_1, λ_2 and λ_4, such that a prescribed percentage of the GPR data (e.g., 95%) satisfies $\left\|\mathbf{G}\mathbf{h}^{\mathrm{est}} - \mathbf{h}^{\mathbf{GPR}}\right\| < \boldsymbol{\varepsilon}^{\mathbf{GPR}}$.~~

~~This can be achieved with different strategies. One option is to fix λ_2 and λ_4, and to vary λ_1 until the condition, mentioned above, is met. Alternatively, it is possible to fix the pairs λ_1/λ_4 or λ_1/λ_2 and to vary λ_2 or λ_4. Choice of the most appropriate strategy depends on the uncertainties associated with the individual contributions in Equation (11).~~

~~The dimension of the system of equations in (11) can be very large, but the matrices **G**, **L**, **B** and **S** are all extremely sparse. Therefore, sparse matrix solvers, such as LSQR (Paige and Saunders, 1982) can solve such systems efficiently for $\mathbf{h}^{\mathbf{est}}$.~~

2.2 Performance tests

For testing the GlaTE inversion algorithm, we investigated glacier ice thickness at three sites in the Swiss Alps (Figure 1~~Figure 1Figure 1Figure 1~~, and Table 1 ~~Table xx~~). The first site is Morteratschgletscher (Figure 1~~Figure 1Figure 1Figure 1~~a). Lying at altitudes between 2050 and 4000 m a.s.l. (Zekollari et al., 2013), the glacier has a typical valley-glacier shape and is located in the Engadin region of Switzerland. In 2015, the tributary glacier Vadret Pers in the east detached from the main trunk of Morteratschgletscher, but we continue to treat both glaciers as a connected system, since the last available outline of the glaciers in 2015 shows the remnant of the former connection. In 2010, the glacier system covered an area of ≈ 15 km^2, and it had a length of ≈ 7.4 km.

The second site, Glacier Plaine Morte (2400-3000 m a.s.l., (Figure 1~~Figure 1Figure 1Figure 1~~b), is the largest plateau glacier in the European Alps (Huss et al., 2013). The surface slope is shallow with an average slope angle~~s~~ of about~~less than~~ ~~6~~4° and a short glacier tongue draining towards the North.

The third site is a cluster of small valley flank and cirque-type glaciers on the eastern flank of the Matter valley (Figure 1~~Figure 1Figure 1Figure 1~~c) below the Dom peak. From North to South, the glaciers are named Hohbärggletscher, Festigletscher, Kingletscher and Weingartengletscher. The Hohbärggletscher is the largest (2800-4500 m a.s.l.) and longest of the group. The individual glaciers were treated as individual flowsheds during the data analysis. The α_{GPR} factor was determined for the entire Dom area.

For all sites, the recorded GPR profiles are shown in Figure 1~~Figure 1Figure 1Figure 1~~. ~~The GPR data are a composite of several campaigns.~~ Most of the data were recorded with the dual polarization system AIR-ETH (Langhammer et al., 2018). On the Glacier Plaine Morte, a grid of profiles was acquired in 2016, and on the Morteratschgletscher and in the Dom Region in 2017. The data were processed as described in Grab et al. (2018), and the bedrock depths and the corresponding ice thicknesses were obtained from the migrated GPR images.

As input data for the glacier models, surface topography and an outline of the individual glaciers was required. As surface topography, we used the swissALTID3D (DTM, Digital Terrain Model Release 2017 © swisstopo (JD100042)). The most recent version, covering the individual glaciers, was extracted and down-sampled to 10 m resolution. The outline represents the extension of the glacier in 2015-2016. DTM and glacier outlines are displayed in Figure 1~~Figure 1Figure 1Figure 1~~. In accordance with Farinotti et al. (2009), we employed mass balance gradients of 0.05 and 0.09 in the accumulation and ablation zones respectively.

As an appropriate measure of the accuracy of the GPR data, we considered a relative (depth-dependent) quantity $\boldsymbol{\varepsilon}^{\mathbf{GPR}} = \left\| \mathbf{h}^{\mathbf{glac}} - \mathbf{h}^{\mathbf{GPR}} \right\| / \left(\mathbf{h}^{\mathbf{GPR}} + h^{\min} \right)$, where $h^{\min}$ is a minimum thickness to avoid unreasonably large relative errors at shallow depths. Values of $\boldsymbol{\varepsilon}^{\mathbf{GPR}} = 0.05$ and $h^{\min} = 5.0$ were judged to be adequate. For all three data sets, we employed $\lambda_4^{\min} = 4.0$, and the prescribed data fit was 95%. This could be achieved with a minimum λ_1/λ_2 ratio of 3.0 (initial values for λ_4 and λ_1/λ_2 were *50.0* and *5.0*).

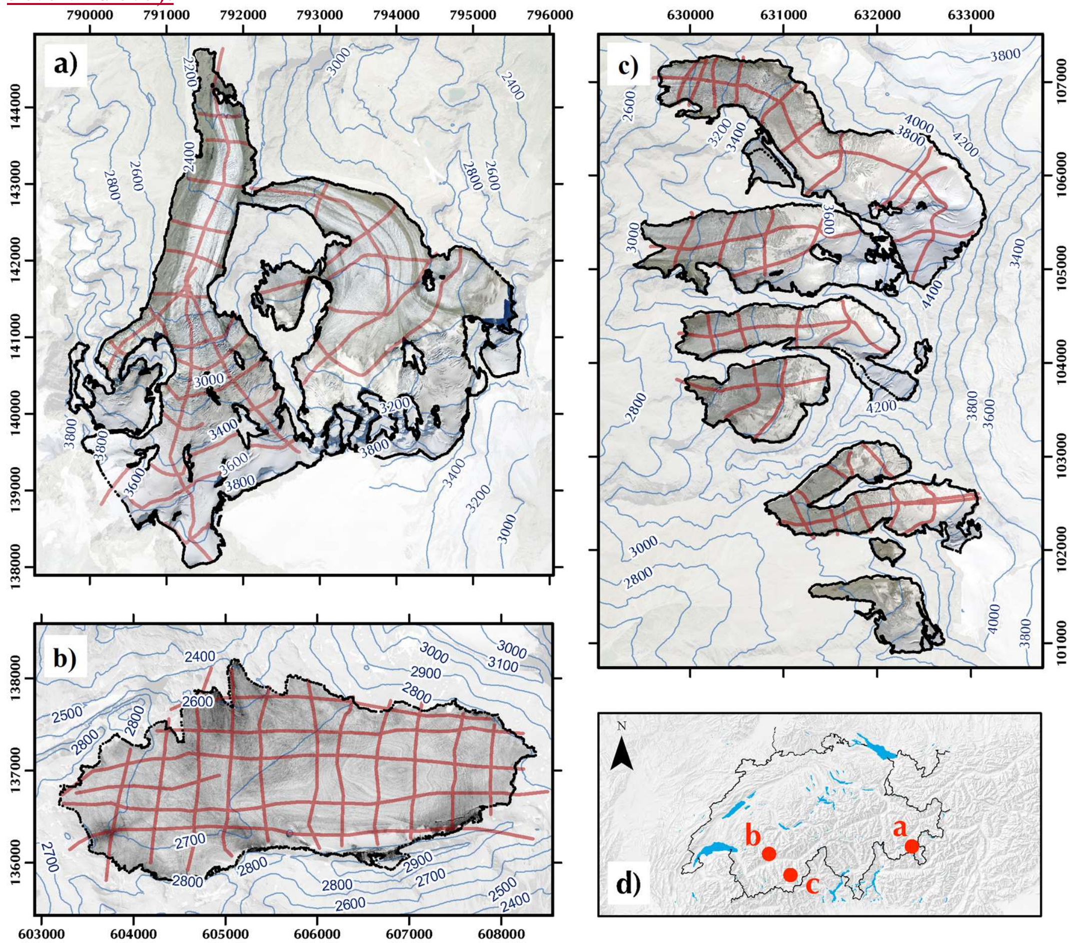

Figure 1: ~~Satellite~~ Orthoimages and surface topography isolines of the glaciers investigated. (a) Morteratschgletscher, (b) Glacier Plaine Morte and (c) Dom region. The Swiss map in the bottom right panel indicates the locations of the glaciers. GPR profiles acquires are shown in red. Orthophotos © 2017 swisstopo (JD100042). Coordinate system: CH1903.

Name	**Area [km^2]**	**Slope ϕ [deg]**	**No. of GPR profiles**	**No. of GPR data points**
Morteratsch	15.3	22	41~~1~~	53,247~~10~~
Plaine Morte	7.4	6	17	36,165~~7.8~~
Dom	9.1~~1.2 8~~	25~~1~~	43~~1~~	34,483~~10~~

Table 1: Characteristics and data sets of glaciers investigated. Slope ϕ denotes the average slope angle.

~~Before applying GlaTE inversions to all field sites, we tested the different options for determining λ_1, λ_2 and λ_4, using the data from Morteratschgletscher. Figure 2 shows the ice thicknesses distributions, (i) when only glaciological constrains are applied ($\mathbf{h}^{glac}$, Figure 2a), and (ii) when only GPR constraints are considered ($\mathbf{h}^{GPR}$, Figure 2b). In the latter case, the thicknesses are obtained by natural neighbor interpolation from the GPR data. Since no extrapolation was performed, not all glacierized regions have an ice thickness estimate. Both images exhibit increased thicknesses in the western glacier, but only the glaciological constraints indicate an overdeepening in the eastern one, thereby indicating that the two models are inconsistent.~~

~~Figure 3 shows the results of the GlaTE inversions using either prescribed λ_1/λ_4 (Figure 3a), λ_1/λ_2 (Figure 3c) or λ_2/λ_4 (Figure 3e) pairs. The corresponding difference plots (Figure 3b, d and f) refer to the deviation of the obtained thickness results compared with the thickness calculated with the glaciological approach. We varied the λ_2 and λ_4 parameters by starting with very high values of 50, and by decreasing them successively until 95% of the GPR data met the condition $\left\|\mathbf{G}\mathbf{h}^{est} - \mathbf{h}^{GPR}\right\| < \boldsymbol{\varepsilon}^{GPR}$, where $\boldsymbol{\varepsilon}^{GPR}$ was estimated to be 5 m. In contrast, we started with a low value of 0.02 for variable λ_1, and increased it successively until 95% of the data were fitted within the error $\boldsymbol{\varepsilon}^{GPR}$. Table 1 summarizes the prescribed and estimated λ values.~~

~~All three inversion strategies (i.e., either varying λ_2, λ_4 or λ_1) yielded comparable results. Although the difference plots with respect to the glaciological model exhibit considerable differences (Figures 3b, 3d and 3f), the general shapes obtained with the glaciological constraints were well preserved in regions where the GPR data coverage was poor. From this first test, we conclude that (i) the GlaTE inversion approach works well, and (ii) that the strategy by which the values of λ are chosen is not critical.~~

Name~~Inversion type~~	~~λ_1 / λ_2~~ final	~~λ_4~~ final	Data fit [%] ~~λ_3~~
Morteratsch ~~λ_1/λ_4 fixed~~	~~1~~	~~0.78~~	~~1~~
Plaine Morte ~~λ_1/λ_2 fixed~~	~~1~~	~~1~~	~~1~~
Dom ~~λ_2/λ_4 fixed~~	~~1.28~~	~~1~~	~~1~~
~~λ_1/λ_4 fixed~~	~~1~~	~~1.56~~	~~1~~
~~λ_1/λ_4 fixed~~	~~1~~	~~0.00~~	~~1~~

Figure 2~~Figure 2Figure 2~~ shows the ice thicknesses distributions, when only glaciological constraints are applied ($\mathbf{h}^{\mathbf{glac}}$, Figure 2~~Figure 2Figure 2~~a), when only GPR constraints are considered ($\mathbf{h}^{\mathbf{GPR}}$, Figure 2~~Figure 2Figure 2~~b), results from the GlaTE algorithm ($\mathbf{h}^{\mathbf{est}}$, Figure 2~~Figure 2Figure 2~~c), and the difference between $\mathbf{h}^{\mathbf{glac}}$ and $\mathbf{h}^{\mathbf{est}}$ (Figure 2~~Figure 2Figure 2~~d). In Figure 2~~Figure 2Figure 2~~b, the thicknesses were obtained by natural neighbor interpolation from the GPR data. Since no extrapolation was performed, not all glacierized regions have an ice thickness estimate. $\mathbf{h}^{\mathbf{glac}}$ ~~-~~and $\mathbf{h}^{\mathbf{GPR}}$ exhibit increased thicknesses in the western glacier, but only the glaciological constraints indicate an overdeepening in the eastern one, thereby indicating that the two models are inconsistent. The results from the GlaTE inversion ($\mathbf{h}^{\mathbf{est}}$, Figure 2~~Figure 2Figure 2~~c) demonstrate that it is possible to find a smooth model that satisfies both, the glaciological and the GPR data constraints.~~*Table 21: Weighting parameters λ employed for the GlaTE inversions shown in Figures 3 and 4. Numbers marked red indicate varying parameters.*~~

~~It is instructive to study the effects of an overly small or large (fixed) λ_4 value. As shown in Table 1, we employed a prescribed value of 10 for λ_4. This value was chosen by trial and error. There was a range of λ_4 values around 10 that yielded similar results (not shown). Choosing very low or high λ_4 values (i.e., $\lambda_4 = 2$ resp. $\lambda_4 = 50$) has a detrimental effect on the results, as shown in Figure 4. For $\lambda_4 = 2$, the inversion fits the ice thicknesses obtained from the GPR data only along the profile lines and maintains the glaciological modeling results in the remaining areas. This produces artificial features in the thickness map (Figure 4a). In contrast, $\lambda_4 = 50$ produces overly smooth images, which is obscuring small-scale variations from the glaciological constraints in regions poorly covered by GPR data (Figure 4e). It is also noteworthy that even with $\lambda_2 = 0$ only approx. 70% of the discrepancies $\left\| \mathbf{G}\mathbf{h}^{\mathbf{est}} - \mathbf{h}^{\mathbf{GPR}} \right\|$ were below $\boldsymbol{\varepsilon}^{\mathbf{GPR}}$ (Figure 5e).~~

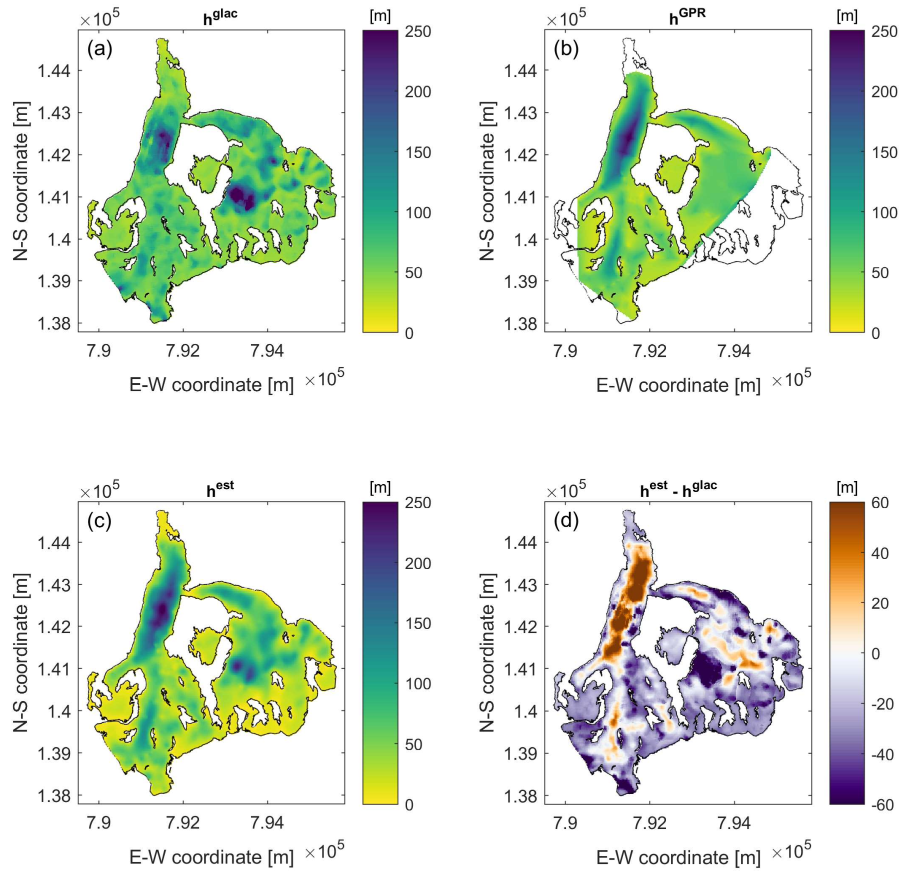

~~*Figure 2: Results from Morteratschgletscher only using (a) glaciological constraints and (b) GPR constraints. Colors indicate ice thickness. Available thickness data obtained from GPR profiles are marked with black lines.*~~

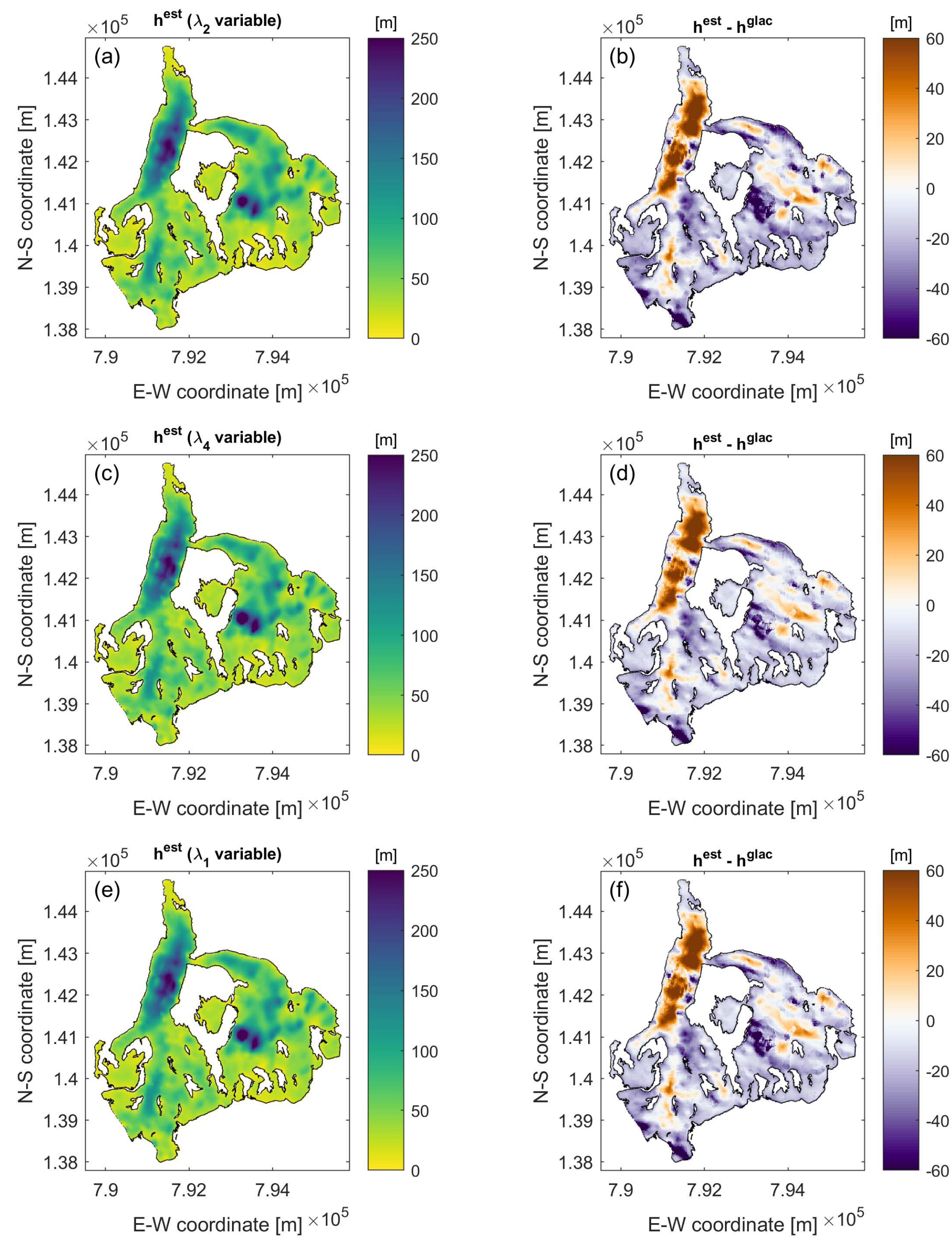

~~*Figure 3: Results from Morteratschgletscher using different strategies for choosing weighting parameters λ (see text for more explanations). Left panels show ice thickness distributions and right panels show differences to glaciological model without GPR constraints (Figure 2a).*~~

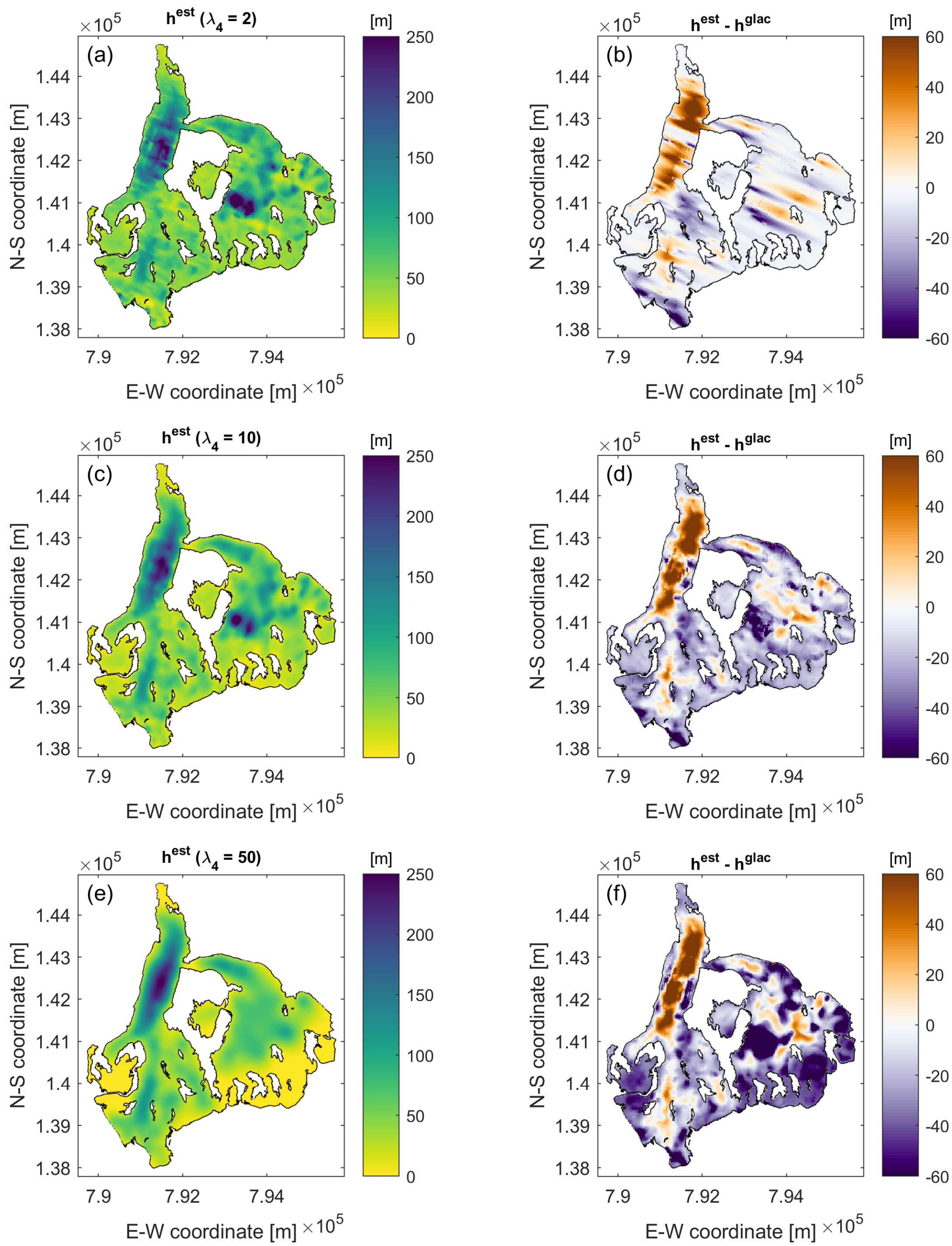

~~*Figure 4: Results from Morteratschgletscher using fixed λ_1 and λ_4 values and varying λ_2. (a) and (b) are the results for $\lambda_4 = 2$, (c) and (d) for $\lambda_4 = 10$ and (e) and (f) for $\lambda_4 = 50$. Left panels show ice thickness distributions and right panels show differences to glaciological model without GPR constraints (Figure 2a).*~~

~~In the following, we consider only the scheme in which λ_1/λ_2 is kept fixed $(\lambda_1=1,\lambda_2=1)$, and λ_4 is varied for analyzing the Glacier Plaine Morte and the Dom region data.~~ The corresponding results ~~are shown in Figures 5 and 6. F~~for the Glacier Plaine Morte are shown in Figure 3: Results from Glacier Plaine Morte only using (a) glaciological constraints or (b) GPR constraints. (c) shows the GlaTE inversion result, and (d) depicts the difference between the results shown in (a) and (c). Colors indicate ice thickness or ice thickness differences. Available thickness data obtained from GPR profiles are marked with black lines in (b).~~Figure 3: Results from Glacier Plaine Morte only using (a) glaciological constraints or (b) GPR constraints. (c) shows the GlaTE inversion result, and (d) depicts the difference between the results shown in (a) and (c). Colors indicate ice thickness or ice thickness differences. Available thickness data obtained from GPR profiles are marked with black lines in (b).Figure 3: Results from Glacier Plaine Morte only using (a) glaciological constraints or (b) GPR constraints. (c) shows the GlaTE inversion result, and (d) depicts the difference between the results shown in (a) and (c). Colors indicate ice thickness or ice thickness differences. Available thickness data obtained from GPR profiles are marked with black lines in (b).~~. ~~, t~~The glaciological model suggests a deep isolated trough slightly east of the center (Figure 3: Results from Glacier Plaine Morte only using (a) glaciological constraints or (b) GPR constraints. (c) shows the GlaTE inversion result, and (d) depicts the difference between the results shown in (a) and (c). Colors indicate ice thickness or ice thickness differences. Available thickness data obtained from GPR profiles are marked with black lines in (b).~~Figure 3: Results from Glacier Plaine Morte only using (a) glaciological constraints or (b) GPR constraints. (c) shows the GlaTE inversion result, and (d) depicts the difference between the results shown in (a) and (c). Colors indicate ice thickness or ice thickness differences. Available thickness data obtained from GPR profiles are marked with black lines in (b).Figure 3: Results from Glacier Plaine Morte only using (a) glaciological constraints or (b) GPR constraints. (c) shows the GlaTE inversion result, and (d) depicts the difference between the results shown in (a) and (c). Colors indicate ice thickness or ice thickness differences. Available thickness data obtained from GPR profiles are marked with black lines in (b).Figure 5~~a). This is not supported by the GPR data, which rather indicate a larger E-W oriented elongated zone of increased thickness (Figure 3: Results from Glacier Plaine Morte only using (a) glaciological constraints or (b) GPR constraints. (c) shows the GlaTE inversion result, and (d) depicts the difference between the results shown in (a) and (c). Colors indicate ice thickness or ice thickness differences. Available thickness data obtained from GPR profiles are marked with black lines in (b).~~Figure 3: Results from Glacier Plaine Morte only using (a) glaciological constraints or (b) GPR constraints. (c) shows the GlaTE inversion result, and (d) depicts the difference between the results shown in (a) and (c). Colors indicate ice thickness or ice thickness differences. Available thickness data obtained from GPR profiles are marked with black lines in (b).Figure 3: Results from Glacier Plaine Morte only using (a) glaciological constraints or (b) GPR constraints. (c) shows the GlaTE inversion result, and (d) depicts the difference between the results shown in (a) and (c). Colors indicate ice thickness or ice thickness differences. Available thickness data obtained from GPR profiles are marked with black lines in (b).Figure 5~~b). Such a feature is also contained in the GlaTE inversion results (Figure 3: Results from Glacier Plaine Morte only using (a) glaciological constraints or (b) GPR constraints. (c) shows the GlaTE inversion result, and (d) depicts the difference between the results shown in (a) and (c). Colors indicate ice thickness or ice thickness differences. Available thickness data obtained from GPR profiles are marked with black lines in (b).~~Figure 3: Results from Glacier Plaine Morte only using (a) glaciological constraints or (b) GPR constraints. (c) shows the GlaTE inversion result, and (d) depicts the difference between the results shown in (a) and (c). Colors indicate ice thickness or ice thickness differences. Available thickness data obtained from GPR profiles are marked with black lines in (b).Figure 3: Results from Glacier Plaine Morte only using (a) glaciological constraints or (b) GPR constraints. (c) shows the GlaTE inversion result, and (d) depicts the difference between the results shown in (a) and (c). Colors indicate ice thickness or ice thickness differences. Available thickness data obtained from GPR profiles are marked with black lines in (b).Figure 5~~c). Furthermore, the glaciological model in Figure 3: Results from Glacier Plaine Morte only using (a) glaciological constraints or (b) GPR constraints. (c) shows the GlaTE inversion result, and (d) depicts the difference between the results shown in (a) and (c). Colors indicate ice thickness or ice thickness differences. Available thickness data obtained from GPR profiles are marked with black lines in (b).~~Figure 3: Results from Glacier Plaine Morte only using (a) glaciological constraints or (b) GPR constraints. (c) shows the GlaTE inversion result, and (d) depicts the difference between the results shown in (a) and (c). Colors indicate ice thickness or ice thickness differences. Available thickness data obtained from GPR profiles are marked with black lines in (b).Figure 3: Results from Glacier Plaine Morte only using (a) glaciological constraints or (b) GPR constraints. (c) shows the GlaTE inversion result, and (d) depicts the difference between the results shown in (a) and (c). Colors indicate ice thickness or ice thickness differences. Available thickness data obtained from GPR profiles are marked with black lines in (b).Figure 5~~a overestimates the ice thickness in the northeastern part of the glacier.

Results from the Dom region show a relatively good match between the glaciological model (Figure 4: Results from Dom region only using (a) glaciological constraints or (b) GPR constraints. (c) shows the GlaTE inversion result, and (d) depicts the difference between the results shown in (a) and (c). Colors indicate ice thickness or ice thickness differences. Available thickness data obtained from GPR profiles are marked with black lines in (b).~~Figure 4: Results from Dom region only using (a) glaciological constraints or (b) GPR constraints. (c) shows the GlaTE inversion result, and (d) depicts the difference between the results shown in (a) and (c). Colors indicate ice thickness or ice thickness differences. Available thickness data obtained from GPR profiles are marked with black lines in (b).Figure 4: Results from Dom region only using (a) glaciological constraints or (b) GPR constraints. (c) shows the GlaTE inversion result, and (d) depicts the difference between the results shown in (a) and (c). Colors indicate ice thickness or ice thickness differences. Available thickness data obtained from GPR profiles are marked with black lines in (b).Figure 6~~a) and the GlaTE inversion result (Figure 4: Results from Dom region only using (a) glaciological constraints or (b) GPR constraints. (c) shows the GlaTE inversion result, and (d) depicts the difference between the results shown in (a) and (c). Colors indicate ice thickness or ice thickness differences. Available thickness data obtained from GPR profiles are marked with black lines in (b).~~Figure 4: Results from Dom region only using (a) glaciological constraints or (b) GPR constraints. (c) shows the GlaTE inversion result, and (d) depicts the difference between the results shown in (a) and (c). Colors indicate ice thickness or ice thickness differences. Available thickness data obtained from GPR profiles are marked with black lines in (b).Figure 4: Results from~~

~~Dom region only using (a) glaciological constraints or (b) GPR constraints. (c) shows the GlaTE inversion result, and (d) depicts the difference between the results shown in (a) and (c). Colors indicate ice thickness or ice thickness differences. Available thickness data obtained from GPR profiles are marked with black lines in (b).~~Figure ~~6~~c). The glaciological model tends to underestimate the maximum thickness in the center of the glacier tongues, and to overestimate the thickness towards the edges (Figure 4: Results from Dom region only using (a) glaciological constraints or (b) GPR constraints. (c) shows the GlaTE inversion result, and (d) depicts the difference between the results shown in (a) and (c). Colors indicate ice thickness or ice thickness differences. Available thickness data obtained from GPR profiles are marked with black lines in (b).~~Figure 4: Results from Dom region only using (a) glaciological constraints or (b) GPR constraints. (c) shows the GlaTE inversion result, and (d) depicts the difference between the results shown in (a) and (c). Colors indicate ice thickness or ice thickness differences. Available thickness data obtained from GPR profiles are marked with black lines in (b).Figure 4: Results from Dom region only using (a) glaciological constraints or (b) GPR constraints. (c) shows the GlaTE inversion result, and (d) depicts the difference between the results shown in (a) and (c). Colors indicate ice thickness or ice thickness differences. Available thickness data obtained from GPR profiles are marked with black lines in (b).~~Figure 6d). The isolated trough structures (ice thickness > 200 m) in the northernmost glacier in the glaciological model (Figure 4: Results from Dom region only using (a) glaciological constraints or (b) GPR constraints. (c) shows the GlaTE inversion result, and (d) depicts the difference between the results shown in (a) and (c). Colors indicate ice thickness or ice thickness differences. Available thickness data obtained from GPR profiles are marked with black lines in (b).~~Figure 4: Results from Dom region only using (a) glaciological constraints or (b) GPR constraints. (c) shows the GlaTE inversion result, and (d) depicts the difference between the results shown in (a) and (c). Colors indicate ice thickness or ice thickness differences. Available thickness data obtained from GPR profiles are marked with black lines in (b).Figure 4: Results from Dom region only using (a) glaciological constraints or (b) GPR constraints. (c) shows the GlaTE inversion result, and (d) depicts the difference between the results shown in (a) and (c). Colors indicate ice thickness or ice thickness differences. Available thickness data obtained from GPR profiles are marked with black lines in (b).~~Figure ~~6~~a) are only partially supported by the GPR data (Figure 4: Results from Dom region only using (a) glaciological constraints or (b) GPR constraints. (c) shows the GlaTE inversion result, and (d) depicts the difference between the results shown in (a) and (c). Colors indicate ice thickness or ice thickness differences. Available thickness data obtained from GPR profiles are marked with black lines in (b).~~Figure 4: Results from Dom region only using (a) glaciological constraints or (b) GPR constraints. (c) shows the GlaTE inversion result, and (d) depicts the difference between the results shown in (a) and (c). Colors indicate ice thickness or ice thickness differences. Available thickness data obtained from GPR profiles are marked with black lines in (b).Figure 4: Results from Dom region only using (a) glaciological constraints or (b) GPR constraints. (c) shows the GlaTE inversion result, and (d) depicts the difference between the results shown in (a) and (c). Colors indicate ice thickness or ice thickness differences. Available thickness data obtained from GPR profiles are marked with black lines in (b).Figure 6~~b) and the GlaTE inversion (Figure 4: Results from Dom region only using (a) glaciological constraints or (b) GPR constraints. (c) shows the GlaTE inversion result, and (d) depicts the difference between the results shown in (a) and (c). Colors indicate ice thickness or ice thickness differences. Available thickness data obtained from GPR profiles are marked with black lines in (b).~~Figure 4: Results from Dom region only using (a) glaciological constraints or (b) GPR constraints. (c) shows the GlaTE inversion result, and (d) depicts the difference between the results shown in (a) and (c). Colors indicate ice thickness or ice thickness differences. Available thickness data obtained from GPR profiles are marked with black lines in (b).Figure 4: Results from Dom region only using (a) glaciological constraints or (b) GPR constraints. (c) shows the GlaTE inversion result, and (d) depicts the difference between the results shown in (a) and (c). Colors indicate ice thickness or ice thickness differences. Available thickness data obtained from GPR profiles are marked with black lines in (b).Figure 6~~c). In the southernmost Weingartengletscher, no data constraints exist (Figure 4: Results from Dom region only using (a) glaciological constraints or (b) GPR constraints. (c) shows the GlaTE inversion result, and (d) depicts the difference between the results shown in (a) and (c). Colors indicate ice thickness or ice thickness differences. Available thickness data obtained from GPR profiles are marked with black lines in (b).~~Figure 4: Results from Dom region only using (a) glaciological constraints or (b) GPR constraints. (c) shows the GlaTE inversion result, and (d) depicts the difference between the results shown in (a) and (c). Colors indicate ice thickness or ice thickness differences. Available thickness data obtained from GPR profiles are marked with black lines in (b).Figure 4: Results from Dom region only using (a) glaciological constraints or (b) GPR constraints. (c) shows the GlaTE inversion result, and (d) depicts the difference between the results shown in (a) and (c). Colors indicate ice thickness or ice thickness differences. Available thickness data obtained from GPR profiles are marked with black lines in (b).Figure 6~~b). The non-zero differences in this part (Figure 4: Results from Dom region only using (a) glaciological constraints or (b) GPR constraints. (c) shows the GlaTE inversion result, and (d) depicts the difference between the results shown in (a) and (c). Colors indicate ice thickness or ice thickness differences. Available thickness data obtained from GPR profiles are marked with black lines in (b).~~Figure 4: Results from Dom region only using (a) glaciological constraints or (b) GPR constraints. (c) shows the GlaTE inversion result, and (d) depicts the difference between the results shown in (a) and (c). Colors indicate ice thickness or ice thickness differences. Available thickness data obtained from GPR profiles are marked with black lines in (b).Figure 4: Results from Dom region only using (a) glaciological constraints or (b) GPR constraints. (c) shows the GlaTE inversion result, and (d) depicts the difference between the results shown in (a) and (c). Colors indicate ice thickness or ice thickness differences. Available thickness data obtained from GPR profiles are marked with black lines in (b).Figure 6~~d) are the result of the smoothing constraints. Here, the thickness estimates from the glaciological model are thus more trustworthy.

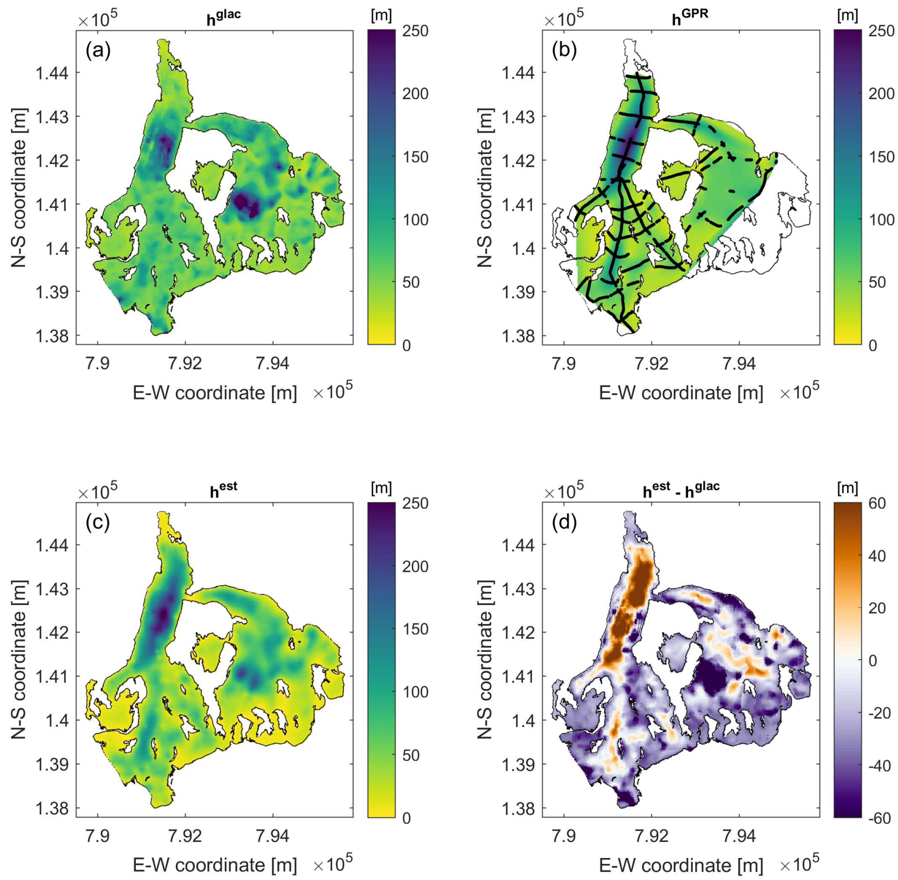

Figure 2: Results from Morteratschgletscher only using (a) glaciological constraints or (b) GPR constraints. (c) shows the GlaTE inversion result, and (d) depicts the difference between the results shown in (a) and (c). Colors indicate ice thickness or ice thickness differences. Available thickness data obtained from GPR profiles are marked with black lines in (b).

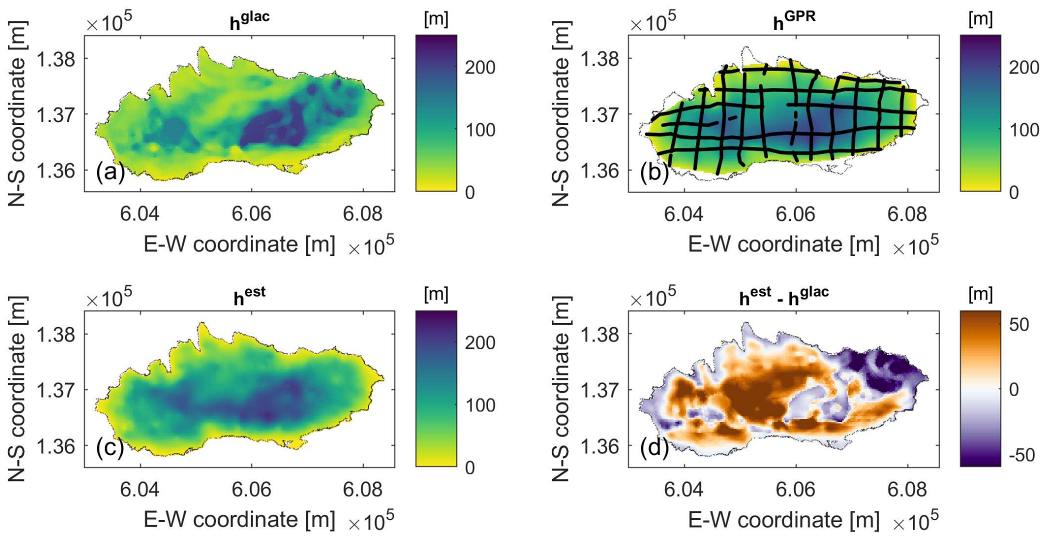

Figure 3: Results from Glacier Plaine Morte only using (a) glaciological constraints or (b) GPR constraints. (c) shows the GlaTE inversion result, and (d) depicts the difference between the results shown in (a) and (c). Colors indicate ice thickness or ice thickness differences. Available thickness data obtained from GPR profiles are marked with black lines in (b).~~*Figure 5: Results from Plaine Morte Glacier. (a) only glaciological constraints, (b) only GPR constraints (available thickness data from GPR profiles marked with black lines), (c) GlaTE inversion, (d) difference between GlaTE inversion and glaciological model.*~~

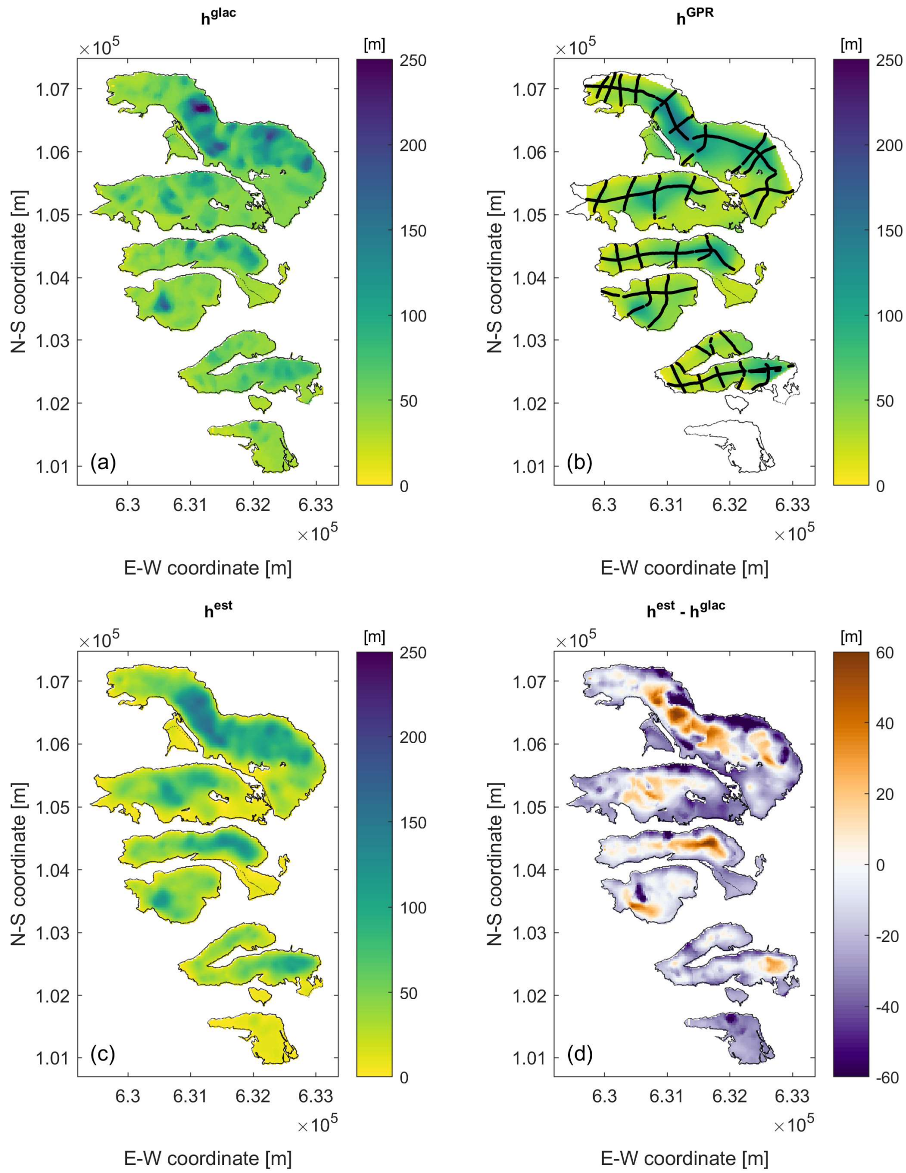

Figure 4: Results from Dom region only using (a) glaciological constraints or (b) GPR constraints. (c) shows the GlaTE inversion result, and (d) depicts the difference between the results shown in (a) and (c). Colors indicate ice thickness or ice thickness differences. Available thickness data obtained from GPR profiles are marked with black lines in (b).~~*Figure 6: Results from the Dom region. (a) only glaciological constraints, (b) only GPR constraints (available thickness data from GPR profiles marked with black lines), (c) GlaTE inversion, (d) difference between GlaTE inversion and glaciological model.*~~

3 Optimized experimental design using GlaTE inversion

All the investigations, described in Section 2, were based on existing GPR data. Their experimental layouts were designed heuristically using experience from prior surveys. Once a glacier model has been established, one may realize that another GPR survey layout may have provided better information. Therefore, a dense survey grid, as employed for 3D seismic reflection campaigns for hydrocarbon exploration for example (e.g., Vermeer, 2003) would be the best choice. This, however, would exceed by far the budgets typically available for glacier investigations.

Optimizing the glaciological constraints with only a limited number of GPR data is a chicken-and-egg problem: identifying the most useful GPR data to be added would require knowledge on where the true ice thickness distribution deviates most from the distribution in the glaciological model, but this would require advanced prior knowledge about the ice thickness that one wants to measure. The problem can be tackled nevertheless by making some specific assumptions (see below).

With our investigations, we address the following questions.

1. Was the experimental geometry and the amount of data acquired in the three investigation areas adequate?
2. Do better experimental layouts exist for constraining the ice thicknesses in a cost-optimized manner?
3. Can some general recommendations be made for designing helicopter-borne GPR surveys on glaciers?

Due to the lack of knowledge on the true ice thicknesses, we assumed that the GlaTE inversion results, shown in Figures 2~~3~~, 33~~35~~ and 44~~46~~ are a good proxy for the actual thickness distributions. Without GPR data, the state of knowledge is represented by the glaciological model (Figures 2~~2~~a, 33~~35~~a and 44~~46~~a). For these models, only 12~~16~~% (Morteratsch), 8~~10~~% (Plaine Morte) and 14~~23~~% (Dom) of the GPR data constraints satisfy the condition $\left\|\mathbf{h}^{\mathbf{glac}} - \mathbf{h}^{\mathbf{GPR}}\right\| / \left(\mathbf{h}^{\mathbf{GPR}} + h^{\min}\right) < \boldsymbol{\varepsilon}^{\mathbf{GPR}}$, and the average ice thickness misfits over the entire glacier area $\left(mean\left(\mathbf{h}^{\mathbf{glac}} - \mathbf{h}^{\mathbf{true}}\right)\right)$ ($\mathbf{h}^{\mathbf{true}}$ = “true” model) are 22~~0~~ m, 32~~25~~ m and 23~~15~~ m for the three data sets, respectively. It should be noted that the glaciological models $\mathbf{h}^{\mathbf{glac}}$ ~~are~~ have been calibrated with α_{GPR}. If no GPR data would have been available, the performance of the glaciological models would have been even worse.

Subsequently, it is analyzed~~,~~ which of the profiles *j (j = 1…nprof (number of profiles))* causes the largest discrepancies between $\mathbf{h}^{\mathbf{GPR}}$ and $\mathbf{h}^{\mathbf{glac}}$. For that purpose we define

(12) $$d_1^{cost} = \max_j \left(\frac{\sum_{i=1}^{i=n_j} P\left(\left|h_{ij}^{GPR} - h_{ij}^{glac}\right| / h_{ij}^{GPR}\right)}{c_j} \right),$$

where index i runs over all n_j data points of profile j. h_{ij}^{GPR} and h_{ij}^{glac} represent the measured and modelled ice thickness at data point i of profile j. The function P is defined as

(13)
$$P(x) := \begin{cases} 1 & if\ x > \varepsilon^{GPR} \\ 0 & if\ x \le \varepsilon^{GPR} \end{cases} .$$

Since longer profiles would be associated with higher (monetary) data acquisition costs, the discrepancy d_1^{cost} is normalized with a cost factor c_j, defined as

(14)
$$c_j = \max\left(len_j, 200\right) ,$$

where len_j represents the length of profile j. This cost function assumes that the acquisition costs increase linearly with profile length, which is realistic, because the helicopter costs are typically charged per minute of flight time. To avoid that overly short profiles would dominate d_1^{cost}, the assumption was made that profiles with len < 200 m would incur the same costs (for such short profiles the flight time is typically governed by positioning the helicopter at the starting point of a profile).

The profile associated with the largest discrepancy d_1^{cost} is expected to offer the largest amount of additional information per unit cost. In this virtual experiment, we assumed that one would acquire this profile and subsequently perform a GlaTE inversion, yielding an improved model $\mathbf{h}^{\mathbf{est}_k}$. Index k indicates the actual state of the experimental design, that is, k is equal to 1, when adding the first profile. Then, the next profile line to be acquired is identified using

(15)
$$d_{k+1}^{cost} = \max_j \left(\frac{\sum_{i=1}^{i=n_j} P\left(\left|h_{ij}^{GPR} - h_{ij}^{est_k}\right| / h_{ij}^{GPR}\right)}{c_j} \right)$$

Repeated application of Equation (15) identifies an optimized sequence for how the profiles should be acquired. Figures 55~~57~~a, 55~~57~~c and 55~~57~~e show the evolution of what we call the “data fit curve”, that is,~~i.e.~~ the evolution of

(16)
$$d_{k+1}^{fit} = \frac{\sum_{j=1}^{j=nprof} \sum_{i=1}^{i=n_j} \hat{P}\left(\left|h_{ij}^{GPR} - h_{ij}^{est_k}\right| / h_{ij}^{GPR}\right)}{\sum_{j=1}^{j=nprof} n_j}$$

with

(17) $$\hat{P}(x) := \begin{cases} 0 & \text{if } x > \varepsilon^{GPR} \\ 1 & \text{if } x \leq \varepsilon^{GPR} \end{cases} .$$

For the Morteratsch ~~and Plaine Morte~~ data, there is an approximately linear increase of the data fit curve. Likewise, we observe a corresponding linear decrease of the average model misfit. As discussed in Maurer et al. (2010), benefit-cost curves, such as the $\boldsymbol{d}^{fit}$ graphs in Figure 5~~Figure 5Figure 5Figure 7~~, typically enter into the area of diminishing returns at some stage, that is, the curves exhibit a characteristic kink and flatten out at larger numbers of profiles. This indicates that it becomes increasingly expensive to obtain additional information. The curve~~s~~ in Figure~~s~~ 55~~57~~a~~ and 7e~~ therefore indicates that the area of diminishing returns was not reached during the Morteratsch ~~and Plain Morte~~ campaigns, and that it would have been useful to acquire more profiles. In contrast, the $\boldsymbol{d}^{fit}$ and average misfit curves for the Plaine Morte and Dom regions ~~(Figure 7e~~Figures5c and 5e) start flattening out, although we do not observe a characteristic kink in the curves. This indicates that it would have ~~been very~~become increasingly expensive to obtain a more accurate ice thickness distribution for the Plaine Morte and Dom field sites.

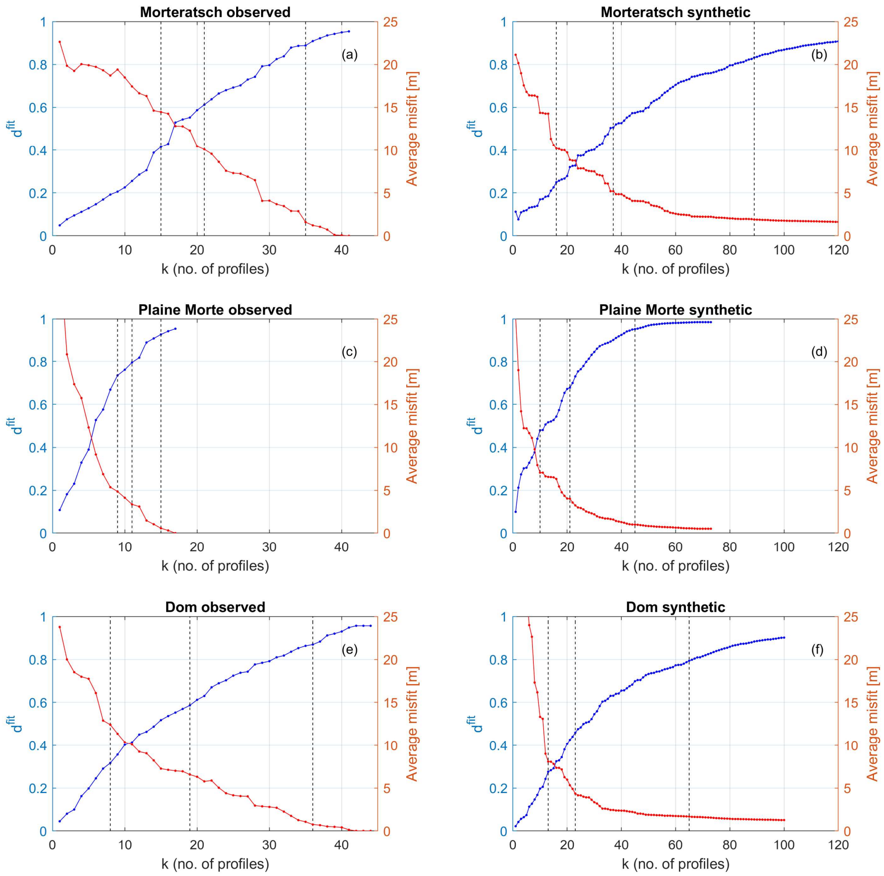

Figure 5557: Evolution of data fit $\mathbf{d}^{\mathbf{fit}}$ *(blue curves) and average data misfit mean*$\left(\mathbf{h}^{\mathrm{est}_k}-\mathbf{h}^{\mathrm{true}}\right)$ *(red curves). Panels a), c) and e) show the results for the observed data, and panels b), d) and f) show the results for the synthetic data generated on a densely spaced grid of hypothetical profiles . Vertical dashes lines indicate the number of profiles required to achieve* d^{fit} *values of 0.5, 0.7 and 0.9 (see also Figures 6668 to 11111113).*

Figures 6668 to 88810 show examples of model misfit plots $\left(\mathbf{h}^{\mathrm{est}_k}-\mathbf{h}^{\mathrm{true}}\right)$ superimposed with the selected profile lines. The corresponding stages of the selection procedure are indicated with black dashed lines in Figures 5557a, 5557c and 5557e. For~~ the~~ Morteratsch~~gletscher~~, profiles are selected preferentially in the western part, because the model fit is already quite good in the eastern region. For Plaine Morte and Dom region~~, it is interesting to note that most N-S profiles are selected before the longer and thus more expensive E-W oriented profiles are considered. In the Dom region~~, no obvious selection patterns can be recognized.

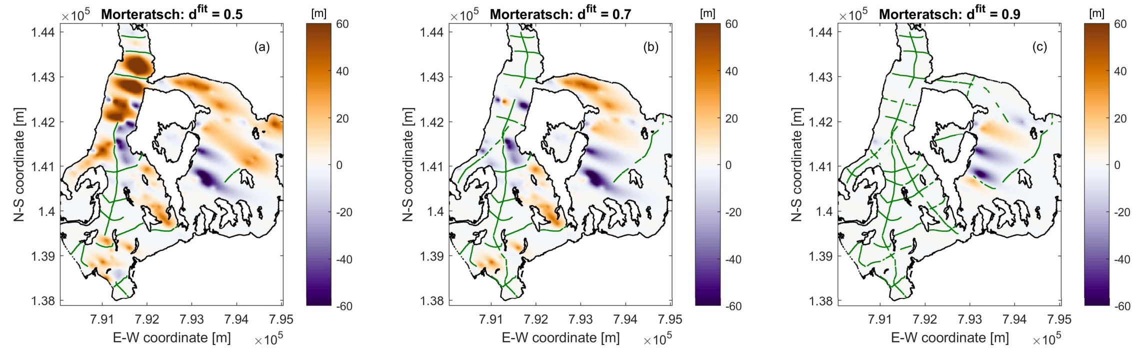

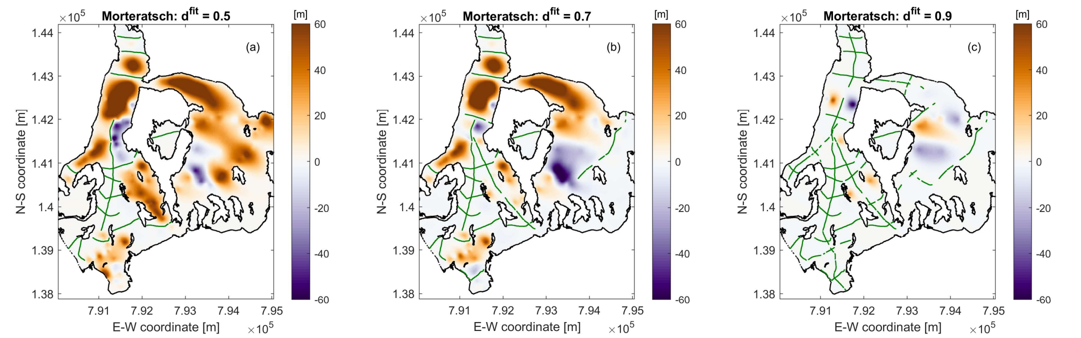

Figure 66~~68~~: Morteratsch model misfit $\mathbf{h}^{\mathbf{true}} - \mathbf{h}^{\mathbf{est}_k}$ *after selected stages of the experimental design procedure using observed data (see also vertical dashed lines in Figure 5~~Figure 5Figure 5Figure 7~~). The selected GPR profiles are superimposed with green lines.*

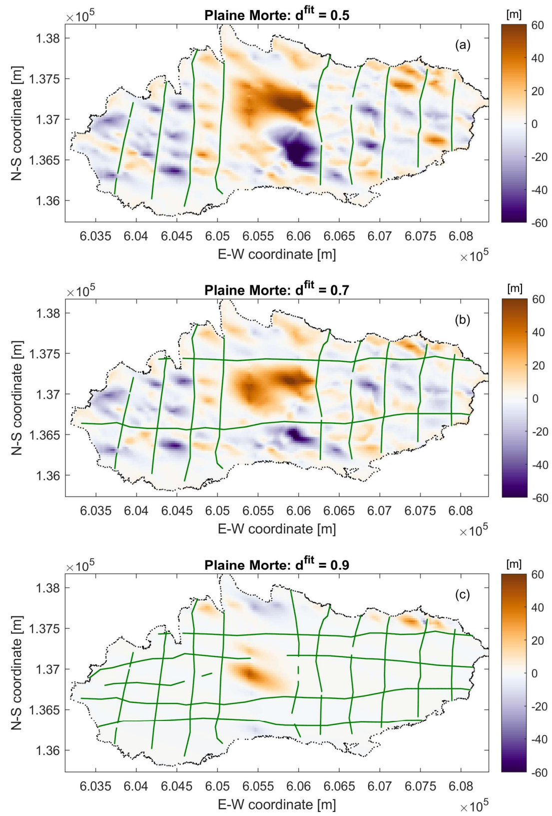
Plaine Morte: d^{fit} = 0.5
(a)
Plaine Morte: d^{fit} = 0.7
(b)
Plaine Morte: d^{fit} = 0.9
(c)
N-S coordinate [m]
E-W coordinate [m]
$\times 10^5$
1.38
1.375
1.37
1.365
1.36
6.035
6.04
6.045
6.05
6.055
6.06
6.065
6.07
6.075
6.08
[m]
60
40
20
0
-20
-40
-60

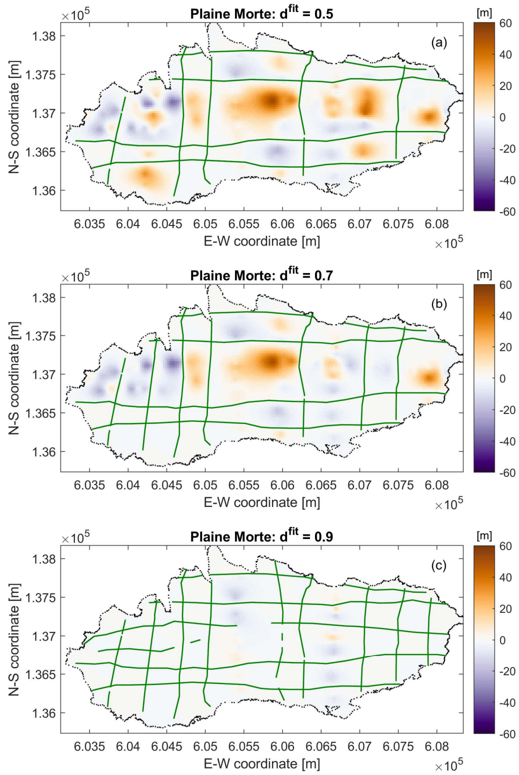

Figure 7~~779~~: Plaine Morte model misfit $\mathbf{h}^{\mathrm{true}} - \mathbf{h}^{\mathrm{est}_k}$ *after selected stages of the experimental design procedure using observed data (see also vertical dashed lines in Figure 5~~Figure 5Figure 5Figure 7~~). The selected GPR profiles are superimposed with green lines.*

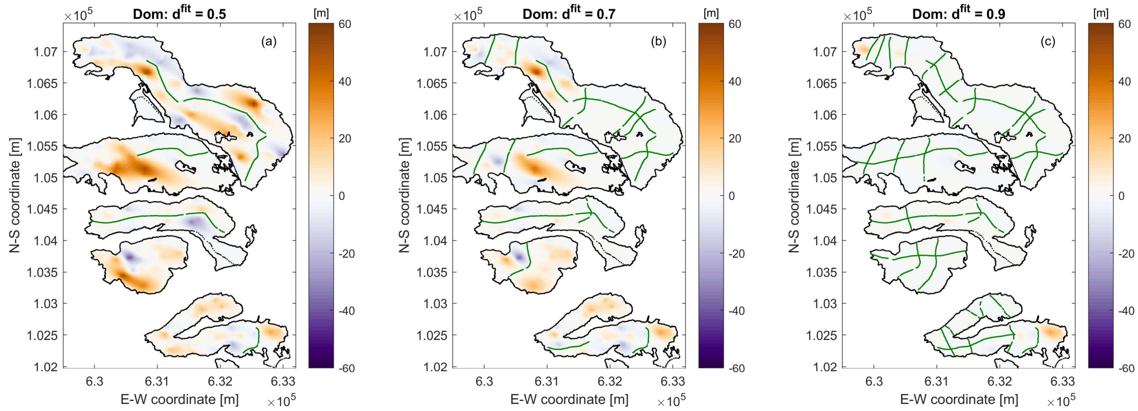

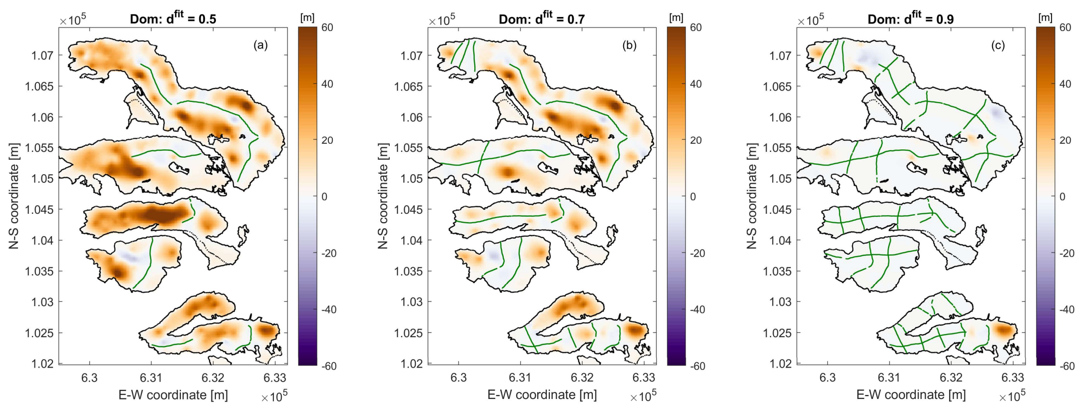

Figure 888~~10~~: Dom model misfit $\mathbf{h}^{true} - \mathbf{h}^{est_k}$ after selected stages of the experimental design procedure using observed data (see also vertical dashed lines in Figure 5~~Figure 5Figure 5Figure 7~~). The selected GPR profiles are superimposed with green lines.

A major limitation of this design experiment is that the "true" model and the recorded GPR profiles have a strong dependency. When all profiles of a particular region are selected, there is a perfect match between $\mathbf{h}_k^{est}$ and $\mathbf{h}^{true}$. However, this is the result of our choice of the "true" model, and thus not indicate that this data set is optimal.

To reduce, at least partially, this dependency, we have generated synthetic data sets that are covering all glacierized areas with a dense grid. We assumed a line spacing of 100 m and an inline sampling interval of 0.5 m, which is representative for the helicopter-borne GPR data that we acquired. With such a comprehensive data set, the experimental design procedure should have more flexibility to choose cost-optimized suites of profiles.

The resulting benefit-cost curves are shown in Figures 55~~57~~b, 55~~57~~d and 55~~57~~f. As expected, the curves start flattening out after selecting a sufficiently large number of profiles. For the Morteratschgletscher (Figure 5~~Figure 5Figure 5Figure 7~~b), it seems to be worthwhile acquiring more than the 43 profiles acquired during the actual experiment. After about 70 profiles, the curve stars flattening out. ~~there is no~~

~~significant benefit observed. Likewise, t~~The curves for the Glacier Plaine Morte (Figure 5~~Figure 5Figure 5Figure 7~~d) indicate clearly that acquiring a larger number of profiles would have been beneficial. After adding about 40 profiles, the $\mathbf{d}^{\mathbf{fit}}$ curve starts flattening out. ~~Only f~~For the Dom region, the amount of profiles chosen for the actual survey seems to be adequate (Figure 5~~Figure 5Figure 5Figure 7~~f). After approx. 40 profiles, the curve is flattening out.~~Note that the decrease in $\mathbf{d}^{\mathbf{fit}}$ at about $k = 8$ and $k = 90$ in Figure 7f are the result of the applied smoothing constraints interfering with the data fit, but this does not affect the general shape of the curve.~~

Using the $\mathbf{d}^{\mathbf{fit}}$ curves in Figure 5~~Figure 5Figure 5Figure 7~~ seems to be a good option for selecting an appropriate number of profiles, but it is also insightful to consider the associated model misfit curves. Figures 5~~557~~b, 5~~557~~d and 5~~557~~f indicate that the average thickness misfit typically approaches a low level,~~ $\varepsilon^{GPR} = 5\%$ is typically reached well~~ before the $\mathbf{d}^{\mathbf{fit}}$ curves start flattening out.

For the experimental design with the synthetic data, Figures 9~~9911~~ to 11~~111113~~ shows examples of model misfit plots $\left(\mathbf{h}^{\mathbf{est}_k} - \mathbf{h}^{\mathbf{true}}\right)$ superimposed with the selected profile lines. In contrast to the selection based on observed data from the Morteratschgletscher (Figure 6~~Figure 6Figure 6Figure 8~~), the design based on the dense synthetic grid (Figure 9~~Figure 9Figure 9Figure 11~~) yields a better balance of profiles among the eastern and western portions of the glacier. This is the consequence of the larger flexibility of choosing profiles with the dense grid. For the Glacier Plaine Morte (Figure 10~~Figure 10Figure 10Figure 12~~), it is interesting to note that almost exclusively N-S oriented profiles were chosen. In contrast, predominantly E-W oriented profiles were chosen for the Dom region (Figure 11~~Figure 11Figure 11Figure 13~~). Both observations are governed primarily by the cost factor c_j in Equation (15).

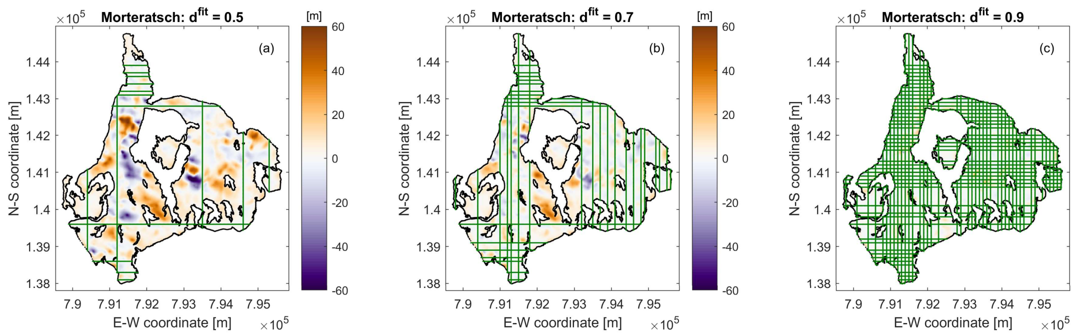

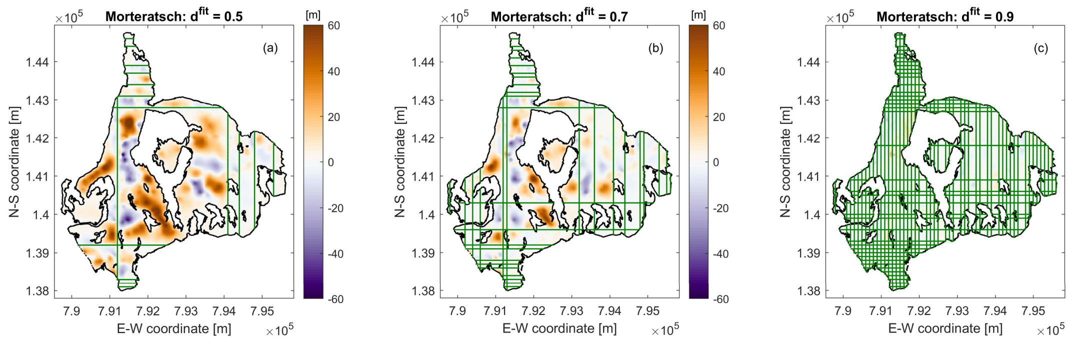

Figure 99~~11~~: Morteratschgletscher model misfit $\mathbf{h}^{\mathbf{true}} - \mathbf{h}^{\mathbf{est}_k}$ *after selected stages of the experimental design procedure using synthetic data (see also vertical dashed lines in Figure 5~~Figure 5Figure 5Figure 7~~). The selected GPR profiles are superimposed with green lines.*

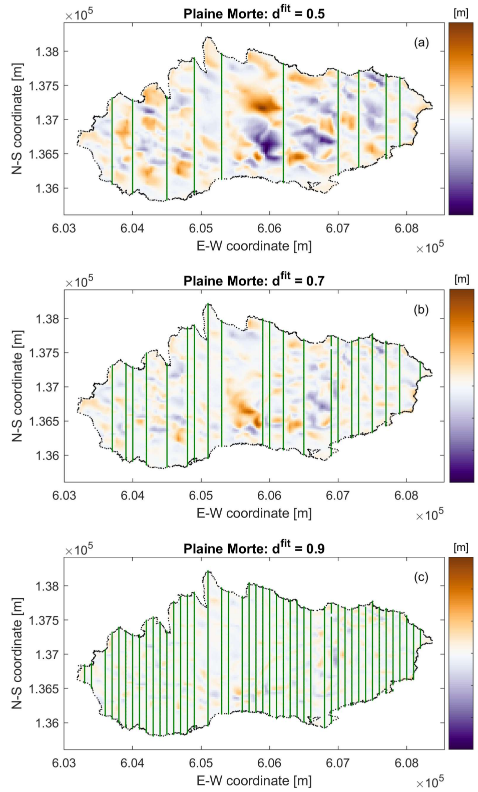

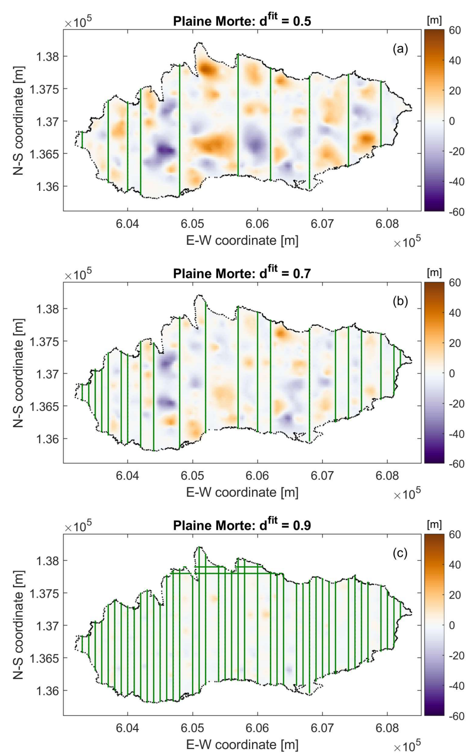

Figure 10~~101012~~: Glacier Plaine Morte model misfit $\mathbf{h}^{true} - \mathbf{h}^{est_k}$ *after selected stages of the experimental design procedure using synthetic data (see also vertical dashed* *lines in Figure 5~~Figure 5Figure 5Figure 7~~). The selected GPR profiles are superimposed with green lines.*

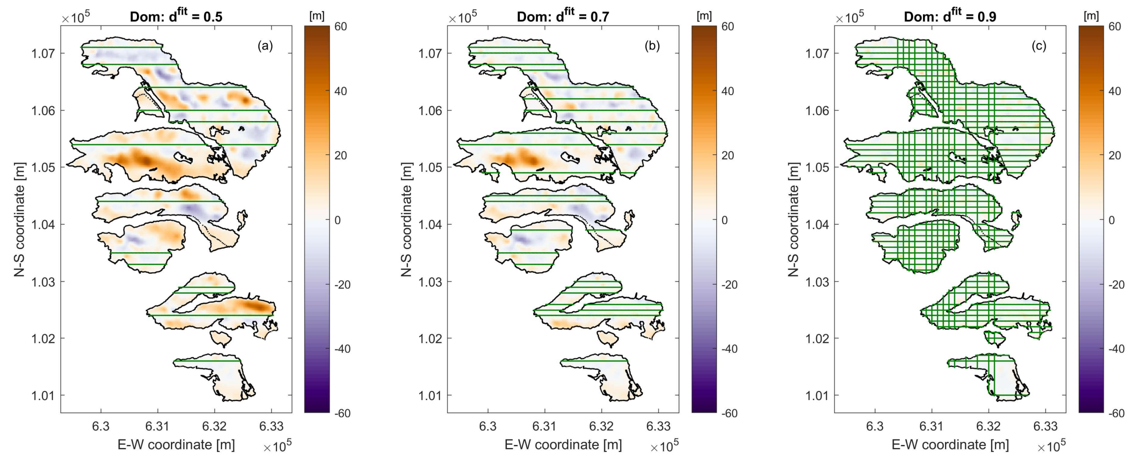

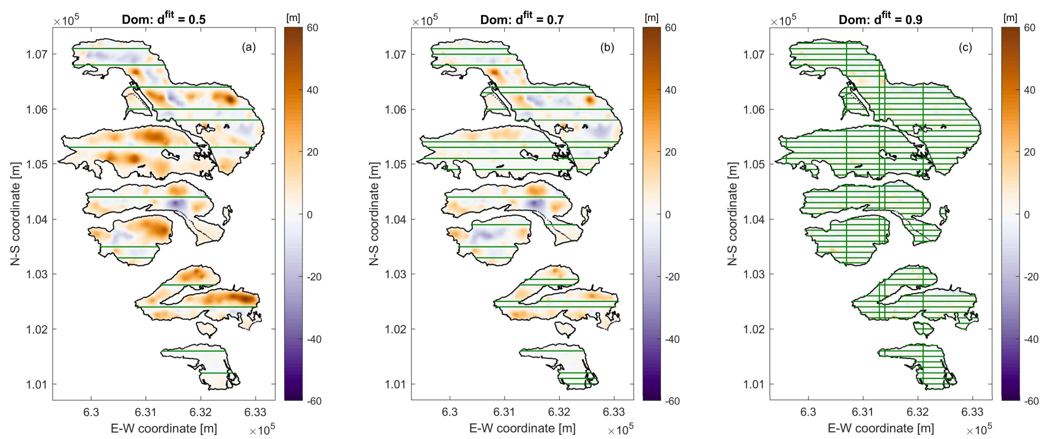

Figure 11~~111113~~: Dom Region model misfit $\mathbf{h}^{true} - \mathbf{h}^{est_k}$ after selected stages of the experimental design procedure using synthetic data (see also vertical dashed lines in Figure 5~~Figure 5Figure 5Figure 7~~). The selected GPR profiles are superimposed with green lines.

4 Discussion and conclusions

The GlaTE inversion scheme presented in this paper offers numerous beneficial features. A benchmark for its capabilities, compared with other methods, will be evaluated in the framework of the ITMIX2 initiative, which is currently ongoing.

Its main advantage is its versatility, as there are several parameters, by which the algorithm can be tuned to the peculiarities of a particular investigation area. However, this is also one of the method’s major drawbacks, since the choice of the control parameters may include a considerable amount of subjectivity. This applies primarily to the choice of the weighting factors λ_1, λ_2 and λ_4. We consider our strategy for determining these factors to be adequate, but other options may work equally well.~~Finding an appropriate value for λ_4^{min} can be particularly awkward, since there is typically no ground-truth information available on the lateral smoothness of the ice thickness distribution. Therefore, we have chosen to keep λ_1 and λ_2 fixed and to determine λ_4 automatically. Quantifying our (relative) confidence in the GPR constraints (λ_1) and glaciological constraints (λ_2) is also a non-trivial task. For this problem, however, some physical arguments may exist. Nevertheless, it might be helpful to repeat the GlaTE inversions with a range of λ_1 / λ_2 ratios and to check the corresponding variations in the resulting models.~~

Another potential problem is the determination of the scaling factor α_{GPR} in Equation (7). It is largely dependent on the available GPR data, and it is assumed that the GPR profiles have a good areal coverage, which might not be always the case. If values for α_{GPR} would be available for a large number of glaciers, a statistical analysis might be used to correlate the values with specific features of the glaciers (e.g., average ~~steepness~~slope, elevation above sea level, size or shape of the glacier, exposure, etc.). This may be helpful in areas, where the GPR data coverage is poor or even non-existent.

In principle, any observations (e.g., boreholes) can be employed as data constraints in Equation (1), but GPR measurements are typically the main source of information. Migration of the GPR data allows the bedrock reflections to be imaged at the correct positions and slopes along a profile, but it is possible that the reflections originated from locations away from the profile lines (off-plane reflections). This may cause systematic errors affecting the reliability of the results. We note, however, that this is not a problem specific to GlaTE, but rather a general issue affecting GPR data acquired on a sparse grid.

As mentioned in Section 2, the system of equations in (11) can be augmented by any linear constraints. An obvious, and in our view particularly useful set of constraints would be offered by surface displacement measurements. They can be obtained from differential satellite images and offer full coverage over a glacier. Such constraints could possibly substitute the smoothness constraints in Equation (11) with a physically more meaningful quantity.

Despite the limitations of our experimental design approach, we judge that our results provided useful insights for designing GPR experiments, and some answers to the questions posed in Section 3 can be provided.

1. *Was the experimental geometry and the amount of data acquired in the three investigation areas adequate?*

   The benefit-cost curves in Figure 5~~Figure 5Figure 5Figure 7~~ indicate that, at least for the Morteratsch ~~and Glacier Plaine Morte~~glacier, it would have been useful to acquire more data.

2. *Do better experimental layouts exist for constraining the ice thicknesses in a cost-optimized manner?*

   The experimental layouts in Figures 6~~668~~ to 11~~111113~~ do not provide unexpected features, but indicate that acquiring a larger number of shorter profiles, instead of recording a few long ones, could be beneficial, but it should be noted that we do not take into account the flight time required to move to the next profiles. This could be significant on glaciers with steep mountain flanks.

3. *Can some general recommendations for designing helicopter-borne GPR surveys on glaciers be made?*

   Based on our results, it is difficult to offer general recommendations. For estimating the overall amount of data to be collected, the benefit-cost curves are most indicative. However, in our case studies they do not flatten out clearly, thereby indicating that it would be worthwhile acquiring more data. When high-precision ice thickness maps are required, it is therefore advisable to acquire as much data as can be afforded.

   It is common practice to acquire crossing profiles, but from the experimental layouts, shown in Figure 10~~Figure 10Figure 10Figure 12~~, it could be concluded that it is not necessary to acquire a large amount of crossing profiles. From a practical point of view, this recommendation cannot be fully supported. When the signal-to-noise ratio of the GPR profiles is poor, it can be difficult to identify the bedrock reflections unambiguously. Due to the importance of crossing profiles, it is judged worthwhile to extend the cost function of the experimental design algorithm, such that crossing profiles are favored.

   It is not realistic to adopt a real-time experimental design strategy (i.e., choosing the next profile based on the results of the previously acquired data), as assumed in our virtual experiments in Section 3. However, if logistically feasible, it might be useful to employ a two-step acquisition strategy. Initially, only a few profiles could be acquired. After analyzing these data sets, regions, where large discrepancies between $\mathbf{h}^{est}$ and $\mathbf{h}^{glac}$ exist, could be identified, and a suitable set of additional profiles could be acquired with a second campaign.

Acknowledgments

We thank Patrick Lathion, Philipp Schaer and Kevin Délèze from GEOSAT SA, Patrick Fauchère from Air Glacier, Hansueli Bärfuss from Heli-Bernina, as well as Lasse Rabenstein and Lino Schmid for acquiring the data. Furthermore, we thank Matthias Huss for fruitful discussions and Daniel Farinotti for an insightful in-house review, which improved the clarity of the manuscript. The manuscript was further improved by the valuable comments of Ben Pelto, Douglas Brinkerhoff and Fabien Maussion. Financial support was provided by ETH Zurich (Grant ETH-15 13-2), the Innosuisse program SCCER-SOE (Swiss competence center for energy research, supply of electricity), and the Swiss Geophysical Commission and ETH Zurich. Finally, we acknowledge the authors of the public-domain Matlab TopoToolbox, which proved to be very useful for this project.

Access to codes and data sets

A Matlab implementation of GlaTE and the test data sets, shown in this paper, can be downloaded from https://gitlab.com/hmaurer/glate .
~~xxx.~~

References

Clarke, G. K., Anslow, F. S., Jarosch, A. H., Radić, V., Menounos, B., Bolch, T., and Berthier, E.: Ice volume and subglacial topography for western Canadian glaciers from mass balance fields, thinning rates, and a bed stress model, J Climate, 26, 4282-4303, 2013.

Constable, S. C., Parker, R. L., and Constable, C. G.: Occam's inversion: A practical algorithm for generating smooth models from electromagnetic sounding data, Geophysics, 52, 289-300, 1987.

Evans, S.: Radio techniques for the measurement of ice thickness, Polar Record, 11, 406-410, 1963.

Farinotti, D., Huss, M., Bauder, A., Funk, M., and Truffer, M.: A method to estimate the ice volume and ice-thickness distribution of alpine glaciers, J Glaciol, 55, 422-430, 2009.

Farinotti, D., Brinkerhoff, D. J., Clarke, G. K., Fürst, J. J., Frey, H., Gantayat, P., Gillet-Chaulet, F., Girard, C., Huss, M., and Leclercq, P. W.: How accurate are estimates of glacier ice thickness? Results from ITMIX, the Ice Thickness Models Intercomparison eXperiment, Cryosphere, 11, 949-970, 2017.

Grab, M., Bauder, A., Ammann, F., Langhammer, L., Hellmann, S., Church, G., Schmid, L., Rabenstein, L., and Maurer, H.: Ice volume estimates of Swiss glaciers using helicopter-borne GPR—an example from the Glacier de la Plaine Morte, 2018 17th International Conference on Ground Penetrating Radar (GPR), 2018, 1-4,

Huss, M., and Farinotti, D.: Distributed ice thickness and volume of all glaciers around the globe, Journal of Geophysical Research: Earth Surface, 117, 2012.

Huss, M., Voinesco, A., and Hoelzle, M.: Implications of climate change on Glacier de la Plaine Morte, Switzerland, Geographica Helvetica, 68, 227-237, 2013.

Iken, A.: Adaption of the hot-water-drilling method for drilling to great depth, Mitteilungen der Versuchsanstalt fur Wasserbau, Hydrologie und Glaziologie an der Eidgenossischen Technischen Hochschule Zurich, 211-229, 1988.

Kamb, B., and Echelmeyer, K. A.: Stress-gradient coupling in glacier flow: I. Longitudinal averaging of the influence of ice thickness and surface slope, J Glaciol, 32, 267-284, 1986.

Langhammer, L., Rabenstein, L., Schmid, L., Bauder, A., Grab, M., Schaer, P., and Maurer, H.: Glacier bed surveying with helicopter-borne dual-polarization ground-penetrating radar, J Glaciol, 1-13, 10.1017/jog.2018.99, 2018.

Linsbauer, A., Paul, F., and Haeberli, W.: Modeling glacier thickness distribution and bed topography over entire mountain ranges with GlabTop: Application of a fast and robust approach, Journal of Geophysical Research: Earth Surface, 117, 2012.

Maurer, H., Curtis, A., and Boerner, D. E.: Recent advances in optimized geophysical survey design, Geophysics, 75, 75A177 – 175A194, 2010.

Maurer, H., Nuber, A., Martiartu, N. K., Reiser, F., Boehm, C., Manukyan, E., Schmelzbach, C., and Fichtner, A.: Optimized Experimental Design in the Context of Seismic Full Waveform Inversion and Seismic Waveform Imaging, in: Advances in Geophysics, Elsevier, 1-45, 2017.

Menke, W.: Geophysical data analysis : discrete inverse theory, Matlab ed., Academic Press, Waltham, MA, 293 p. pp., 2012.

Morlighem, M., Rignot, E., Seroussi, H., Larour, E., Ben Dhia, H., and Aubry, D.: A mass conservation approach for mapping glacier ice thickness, Geophys Res Lett, 38, 2011.

Morlighem, M., Rignot, E., Mouginot, J., Seroussi, H., and Larour, E.: High-resolution ice-thickness mapping in South Greenland, Annals of Glaciology, 55, 64-70, 2014.

Nye, J.: A method of calculating the thicknesses of the ice-sheets, Nature, 169, 529-530, 1952.

Paige, C. C., and Saunders, M. A.: Lsqr - an Algorithm for Sparse Linear-Equations and Sparse Least-Squares, Acm T Math Software, 8, 43-71, 1982.

Rutishauser, A., Maurer, H., and Bauder, A.: Helicopter-borne ground-penetrating radar investigations on temperate alpine glaciers: A comparison of different systems and their abilities for bedrock mapping, GEOPHYSICS, 81, WA119-WA129, doi:10.1190/geo2015-0144.1, 2016.

Steinhage, D., Nixdorf, U., Meyer, U., and Miller, H.: New maps of the ice thickness and subglacial topography in Dronning Maud Land, Antarctica, determined by means of airborne radio-echo sounding, Annals of Glaciology, 29, 267-272, 1999.

Vermeer, G. J.: 3d seismic survey design optimization, The Leading Edge, 22, 934-941, 2003.

Watts, R. D., and England, A. W.: Radio-echo sounding of temperate glaciers: ice properties and sounder design criteria, J Glaciol, 17, 39-48, 1976.

Zekollari, H., Huybrechts, P., Fürst, J., Rybak, O., and Eisen, O.: Calibration of a higher-order 3-D ice-flow model of the Morteratsch glacier complex, Engadin, Switzerland, Annals of Glaciology, 54, 343-351, 2013.